Genetic Modifier Screens in Drosophila Demonstrate a Role for Rho1 Signaling in Ecdysone-Triggered Imaginal Disc Morphogenesis

Robert E. Ward,[1] Janelle Evans and Carl S. Thummel[2]

Howard Hughes Medical Institute, Department of Human Genetics, University of Utah School of Medicine, Salt Lake City, Utah 84112-5331

Manuscript received March 13, 2003
Accepted for publication June 3, 2003

ABSTRACT

Drosophila adult leg development provides an ideal model system for characterizing the molecular mechanisms of hormone-triggered morphogenesis. A pulse of the steroid hormone ecdysone at the onset of metamorphosis triggers the rapid transformation of a flat leg imaginal disc into an immature adult leg, largely through coordinated changes in cell shape. In an effort to identify links between the ecdysone signal and the cytoskeletal changes required for leg morphogenesis, we performed two large-scale genetic screens for dominant enhancers of the malformed leg phenotype associated with a mutation in the ecdysone-inducible *broad* early gene (br^1). From a screen of >750 independent deficiency and candidate mutation stocks, we identified 17 loci on the autosomes that interact strongly with br^1. In a complementary screen of ~112,000 F_1 progeny of EMS-treated br^1 animals, we recovered 26 mutations that enhance the br^1 leg phenotype [*E(br)* mutations]. *Rho1*, *stubbloid*, *blistered* (*DSRF*), and *cytoplasmic Tropomyosin* were identified from these screens as br^1-interacting genes. Our findings suggest that ecdysone exerts its effects on leg morphogenesis through a Rho1 signaling cascade, a proposal that is supported by genetic interaction studies between the *E(br)* mutations and mutations in the Rho1 signaling pathway. In addition, several *E(br)* mutations produce unexpected defects in midembryonic morphogenetic movements. Coupled with recent evidence implicating ecdysone signaling in these embryonic morphogenetic events, our results suggest that a common ecdysone-dependent, Rho1-mediated regulatory pathway controls morphogenesis during the two major transitions in the life cycle, embryogenesis and metamorphosis.

MORPHOGENETIC movements define the body plan of metazoan animals. Gastrulation, neural tube formation, limb development, and organogenesis all depend on precisely timed, coordinated cell shape changes and cell rearrangements. In certain developmental contexts, endocrine signals provide temporal cues and also aid in the proper coordination of these morphogenetic events. For example, estrogen is required for mammary epithelial growth and ductal morphogenesis (Bocchinfuso *et al.* 2000), whereas thyroid hormone coordinates the massive tissue rearrangements that occur during amphibian metamorphosis (Tata 1999). Despite the importance of endocrine signaling in developmental programs, however, the mechanisms by which hormonal signals are transduced to the cellular machinery required for morphogenesis remain largely undefined.

Development of the adult leg in Drosophila provides an ideal model system for characterizing the molecular mechanisms of hormone-triggered morphogenesis. In Drosophila, the adult legs are derived from imaginal discs that are specified during embryogenesis and set aside as discrete clusters of diploid cells that undergo extensive proliferation and patterning during larval development. At the end of the third larval instar each of the six leg imaginal discs consists of a single-layered columnar epithelium that is covered and apposed by a squamous peripodial epithelium. Transformation of this disc epithelium into an immature adult leg is triggered by a pulse of 20-hydroxyecdysone (hereafter referred to as ecdysone), the steroid hormone that directs the major developmental transitions in the Drosophila life cycle (Mandaron 1970; Fristrom *et al.* 1973; Riddiford 1993). In response to the late larval ecdysone pulse, the leg imaginal discs elongate in the proximal-distal axis as the animal pupariates and initiates metamorphosis (Fristrom and Fristrom 1993; von Kalm *et al.* 1995). The leg imaginal discs evert rapidly at ~5 hr after puparium formation, bringing them to the outside of the puparium (Robertson 1936; Ward *et al.* 2003). The proximal regions of the discs then fuse with other thoracic and cephalic discs to contribute to the formation of a rudimentary adult fly. Remarkably, leg elongation and eversion can be recapitulated in cultured discs that are exposed to physiologically relevant levels of ecdysone, demonstrating a key role for the hormone in coordinating these morphogenetic events (Martin and Schneider 1978).

Ecdysone exerts its effects primarily at the level of gene regulation (Ashburner *et al.* 1974). Ecdysone binds to

[1]*Present address:* Department of Molecular Biosciences, University of Kansas, 1200 Sunnyside Ave., Lawrence, KS 66045-7534.

[2]*Corresponding author:* Howard Hughes Medical Institute, University of Utah, 15 N. 2030 East, Rm. 5100, Salt Lake City, UT 84112-5331. E-mail: carl.thummel@genetics.utah.edu

its receptor, a heterodimer of the Ecdysone receptor (EcR) and Ultraspiracle, directly inducing the transcription of primary-response early genes (Riddiford *et al.* 2000). Some of these early genes encode transcription factors that regulate large batteries of secondary-response late genes, thought to direct the appropriate spatial and temporal biological responses to the hormone (Thummel 1996). One such ecdysone-inducible early gene is the *Broad-Complex* (*BR-C*), which encodes a family of zinc-finger transcription factors (DiBello *et al.* 1991). Genetic studies have defined three distinct genetic functions for *BR-C*, of which the *broad* (*br*) function is essential for leg imaginal disc morphogenesis (Belyaeva *et al.* 1980; Kiss *et al.* 1988). Specifically, the leg discs in amorphic br^5 mutant prepupae fail to elongate or evert and appear to arrest at a stage similar to that of a wild-type disc at puparium formation, although the animal continues to develop and makes an apparent attempt to pupate at ~18 hr after puparium formation (Kiss *et al.* 1988; Ward *et al.* 2003). In contrast, mutations of the hypomorphic br^1 allele display only a weakly penetrant malformed leg phenotype in adult flies (Kiss *et al.* 1988).

A number of molecular, biochemical, and genetic approaches have been employed to characterize leg disc morphogenesis. These studies have revealed that elongation and eversion of the leg imaginal discs occur in the absence of cell proliferation, largely in response to changes in cell shape (Graves and Schubiger 1982; Condic *et al.* 1991). These directed cell shape changes appear to contribute to the elongation of the disc in the proximal-distal axis while affecting a contraction in the circumferential dimension, effectively converting the flat imaginal disc into a rudimentary adult leg over the course of several hours (von Kalm *et al.* 1995). A central role for the actin cytoskeleton in driving leg morphogenesis is supported by earlier work by Fristrom and Fristrom (1975) demonstrating that ecdysone-induced elongation and eversion is reversibly inhibited by cytochalasin B. Several studies have also implicated an important role for proteases in imaginal disc morphogenesis during prepupal development (Poodry and Schneiderman 1971; Fekete *et al.* 1975; Pino-Heiss and Schubiger 1989; Birr *et al.* 1990; Fessler *et al.* 1993).

A genetic approach for investigating imaginal disc morphogenesis was employed by Beaton *et al.* (1988), who took advantage of the sensitized genetic background provided by the hypomorphic *BR-C* allele, br^1. Screening through a collection of recessive mutations that produce leg defects, they identified *Stubble/stubbloid* (*Sb/sbd*), which encodes an apparent type II transmembrane serine protease (Appel *et al.* 1993), as a br^1-interacting gene. Subsequently, Gotwals and Fristrom (1991) conducted a small-scale screen of 19,000 randomly mutagenized F_1 animals to identify dominant modifiers of the malformed leg phenotype associated with this mutation. They identified one allele each of *Sb/sbd* and *zipper* (*zip*), which encodes nonmuscle myosin heavy chain. The identification of a chemomechanical motor protein that facilitates contraction of the actin cytoskeleton and an extracellular protease demonstrated the utility of their screen and supported the notion that events at the actin cytoskeleton are critically important for leg morphogenesis.

In this study we expand upon the original Gotwals and Fristrom screen to identify links between the ecdysone signal and the cytoskeletal machinery that drives leg morphogenesis. Two independent screens were undertaken for dominant enhancers of the malformed leg phenotype associated with the br^1 mutation, using either a collection of autosomal chromosomal deficiencies or random methanesulfonic acid ethyl ester (EMS)-generated mutants. From these screens we identified 17 loci on the autosomes that interact with br^1 and we isolated 26 EMS-induced br^1-interacting mutations. Included in this collection of br^1-interacting genes are those encoding the small GTPase Rho1, the Drosophila serum response factor (SRF) transcription factor Blistered (Bs), a cytoplasmic isoform of Tropomyosin1 (cTm), and the Sb/sbd protease. These results imply an important role for Rho1 signaling in leg disc morphogenesis, a notion that we support by genetic interaction studies between the EMS-generated mutations and previously characterized mutations in the Rho1 signaling pathway. In addition, we observe defects in midembryonic morphogenetic movements in animals bearing some of the EMS-induced mutations, suggesting that common regulatory mechanisms drive morphogenesis at different stages in the life cycle.

MATERIALS AND METHODS

Drosophila stocks: All Drosophila stocks were maintained on corn meal/yeast/molasses/agar media in a room maintained at a constant temperature of 21°. The deficiency and *P*-element-insertion stocks used in this study were obtained from the Bloomington Drosophila Stock Center at Indiana University (Bloomington, IN). The $zip^{E(br)}$, $Rho^{J3.8}$, and $Rho^{E3.10}$ stocks were obtained from S. Halsell (James Madison University; Gotwals and Fristrom 1991; Halsell *et al.* 2000). The $RhoGEF2^{11\text{-}3}$ and $zip^{33\text{-}1}$ stocks were obtained from L. von Kalm (University of Central Florida; Bayer *et al.* 2003, this issue). The cTm^{eg9} and cTm^{er4} stocks were obtained from D. Kiehart (Duke University; Erdelyi *et al.* 1995). Unless otherwise stated, genetic experiments were conducted in a room controlled at a constant temperature of 21° because the genetic interactions observed between br^1 and both *Sb/sbd* and *zip* are cold sensitive (Beaton *et al.* 1988; Gotwals and Fristrom 1991).

EMS mutagenesis and screening: Twenty cohorts, each consisting of 30 3- to 5-day-old br^1 males, were treated with 25 mM EMS. Each cohort was mated to 30 br^1 virgin females. Mutagenized males were subsequently mated to a second set of br^1 virgin females to produce two broods of progeny. All progeny were maintained in bottles at 21°. In the F_1 generation, all flies showing malformed legs were backcrossed to br^1 males or females as appropriate. In the F_2 and subsequent generations, sibling flies showing malformed legs were mated *inter se* in an effort to remove unlinked second-site mutations

by free recombination. Starting at the F_5 generation, *inter se* crosses producing ~10% or more malformed progeny were mapped and balanced using the mapping stocks *br*[1]*;Sco/Cyo* and *br*[1]*;T(2;3)ap*[Xa]*/TM6B*. The *br*[1] mutation was subsequently outcrossed leaving balanced *Enhancer of br* [*E(br)*] stocks. Complementation tests were conducted on *E(br)* stocks that mapped to the same chromosome.

Deficiency screen: Dominant genetic interaction tests with *br*[1] were performed by mating five to seven *br*[1] virgin females to five to seven deficiency- or specific mutation-bearing heterozygous males in vials containing standard Drosophila medium. After 3 days the adults were transferred to fresh vials and, subsequently, to a third vial after two additional days. Newly eclosing F_1 flies were separated by genotype and examined for malformed legs each day for a total of 10 days. Second-site noncomplementation (SSNC) tests with *br*[5] were performed in a similar manner, except that *y br*[5]*/Binsn* females were used and the crosses were maintained in an incubator at 25°.

EMS screen: Dominant genetic interaction tests between *br*[1] and the *E(br)* mutations were performed at 21° as described above, using males of the genotype *br*[1]*/Y;E(br)/CyO* or *br*[1]*/Y;E(br)/TM6B*. Two vials were scored for each *E(br)* line in the experiment reported in Table 3. SSNC tests between *br*[5] and the *E(br)* mutations were performed at 25° as described above using *y br*[5]*/Binsn* virgin females and *w*[1118]*/Y;E(br)/CyO* or *w*[1118]*/Y;E(br)/TM6B* males. SSNC tests between *E(br)* mutations and Rho1 pathway mutations were performed by mating five to seven *w*[1118]*;E(br)/CyO* or *w*[1118]*;E(br)/TM6B* virgin females to five to seven heterozygous mutant males. The crosses were maintained at 21° and three vials for each cross were examined in the manner described above. In some cases the reciprocal cross was also performed.

Complementation tests were performed by mating five to seven *w*[1118]*;E(br)/CyO* or *w*[1118]*;E(br)/TM6B* virgin females to five to seven heterozygous mutant males. Crosses were maintained in an incubator at 25°. The adults were transferred to fresh vials after 3 days. Newly eclosing F_1 flies were separated into genotypic classes and counted each day for a total of 7 days. In some cases the reciprocal cross was also performed.

Meiotic mapping of the *E(br)* mutations was performed by mating *br*[1]*;E(br)/CyO* or *br*[1]*;E(br)/TM6B* virgin females to *br*[1]*/Y;b pr c px sp* or *br*[1]*/Y;ru th st ri roe p e ca* males, respectively. In the F_1 generation, virgin females of the genotypes *br*[1]*;E(br)/b pr c px sp* or *br*[1]*;E(br)/ru th st ri roe p e ca* were mated to *br*[1]*/Y;b pr c px sp* or *br*[1]*/Y;ru th st ri roe p e ca* males, respectively. In the F_2 generation, all animals bearing malformed legs [and therefore likely containing the *E(br)* mutation] were examined for the presence of recessive markers. Recombination distances were calculated between the *E(br)* mutation and each recessive marker, and the map position of the *E(br)* mutation was determined using values from the two or three closest recessive markers. From 150 to 400 informative recombination events were scored for each *E(br)* mutation.

Lethal-phase analysis: Embryonic lethality was determined by collecting 0- to 2-hr embryos from *E(br)/Cyo, P{w*[+]*, ActGFP}* or *E(br)/TM6B, P{w*[+]*, UbiGFP}* stocks. The embryos were aged at 25° for 15 hr and dechorionated in 50% bleach, and homozygous *E(br)* embryos were identified and separated on the basis of absence of green fluorescent protein (GFP) expression. The homozygous mutant embryos were allowed to develop at 25° until ~48 hr after egg laying, at which point the dead embryos were counted and mounted in Hoyer's medium (Ashburner 1989) on microscope slides. Embryonic lethality was calculated as (number of dead embryos/number of total mutant embryos) × 100. Thirty to 60 *E(br)* mutant embryos were tested in each experiment and all *E(br)* stocks were tested in triplicate. The mean and standard error (SE) of embryonic lethality were calculated for each *E(br)* stock. Cuticle preparations were examined for terminal phenotypes. Larval lethality was determined by collecting non-GFP-expressing first instar larvae derived from *E(br)/Cyo, P{w*[+]*,ActGFP}* or *E(br)/TM6B, P{w*[+]*,UbiGFP}* stocks. Seventy-five to 100 mutant larvae were placed into vials containing standard Drosophila medium that had been lightly tilled and overlaid with fresh yeast paste. The larvae were aged for 7–10 days at 25°, at which point the number of pupae were counted. Larval lethality was calculated as [(number of total larvae − number of pupae)/number of total larvae] × 100. Experiments were done in triplicate and the mean and SE of larval lethality were calculated for each *E(br)* stock.

Embryonic and adult specimen preparations: The devitellinized embryonic cuticles shown in Figure 4 were prepared by collecting unhatched embryos from *E(br)*/CyO or *E(br)*/TM6B stocks 48 hr after egg laying at 25°. The embryos were dechorionated in 50% bleach and devitellinized in a 1:1 mixture of heptane: 90% MeOH, 50 mm EGTA, pH 8.0. The embryos were then mounted in One-Step mounting medium (2:1:1 glacial acetic acid:CMCP10:85% lactic acid) on microscope slides. Adult leg cuticles were prepared by dissecting leg pairs from the third thoracic segment of *w*[1118], *br*[1]*;E(br)/CyO* or *br*[1]*;E(br)/TM6B* males in PBS, clearing them overnight in 10% KOH, and mounting them in Euporal on microscope slides. Images of the embryonic and adult leg cuticles were captured on either a Cool Snap or a SensiCamQE high performance digital CCD camera mounted on a Zeiss Axiophot microscope. Images of the dorsal thoraces from *sbd*[E(br)228] and *sbd*[E(br)228]/+ animals were captured on a Cool Snap digital CCD camera mounted on a Leica stereomicroscope. Indirect immunofluorescence analysis of *E(br)165* embryos was performed by collecting embryos from *E(br)165/CyO* parents at 25° for 2 hr, aging the embryos for an additional 19 hr, and then fixing and staining the embryos as described (Fehon *et al.* 1991). Anti-Coracle mAb C615-16B was used at a dilution of 1:250. Optical sections were captured with a Bio-Rad (Richmond, CA) MRC1024 confocal laser mounted on a Zeiss Axioplan microscope. All digital images were cropped and adjusted for brightness and contrast in Adobe Photoshop.

RNA isolation and Northern blot analysis: Progeny from a cross of *y br*[5]*/Binsn* × *Binsn/Y* were staged on standard Drosophila media supplemented with 0.1% bromophenol blue as described in Andres and Thummel (1994). Total RNA was isolated by direct phenol extraction from leg imaginal discs dissected from staged *y br*[5]*/Y* and *Binsn/Y* males. Approximately 9 μg of total RNA per sample was separated by formaldehyde agarose gel electrophoresis and transferred to a nylon membrane. The membrane was hybridized and stripped as described by Karim and Thummel (1991). Generation of probe fragments for *BR-C* (core), *ImpE3*, and *rp49* is described in Andres and Thummel (1994) and for *Sb* in D'Avino and Thummel (1998). A probe to detect *Rho1* was generated by PCR amplification of a 581-bp fragment from a late third instar larval random-primed cDNA collection (T. Kozlova, personal communication) using the primer set 5′-AACTTC CAATGACGACGATTCGC-3′ and 5′-GCAAAAGGCATCTGG TCTTCTTCC-3′. A probe to detect *bs* was generated by PCR amplification of a 429-bp fragment from a late third instar larval random-primed cDNA collection (T. Kozlova, personal communication) using the primer set 5′-CGTTGAGTGTTT TCTGTGTGG-3′ and 5′-CTGGGAGGCGTGCTGTGGG-3′. A probe to detect *Rho kinase* was generated by PCR amplification of a 569-bp fragment from cDNA LD36258 (Research Genetics, Birmingham, AL) using the primer set 5′-CGAAATAA AATAAGTGCAACGCGC-3′ and 5′-CATTGCTGGACACCAC TTGGCC-3′. A probe to detect *RhoGEF2* was generated by PCR amplification of a 588-bp fragment from cDNA SD04476 (Research Genetics) using the primer set 5′-CGTCGTGT

GCGTGTTGATGGCG-3′ and 5′-GACGGGCCTGCAGATGT CGC-3′. Specific probes were labeled by random priming of gel-purified fragments (Stratagene, La Jolla, CA).

RESULTS

Screening autosomal deficiency stocks for genetic interactions with *br*: As a first step toward identifying loci that function with *br* to direct leg morphogenesis, we screened through an ordered collection of chromosomal deficiency stocks from the second and third chromosomes. We screened for deficiencies that exert a dominant increase in the penetrance of the malformed leg phenotype associated with the weakly hypomorphic br^1 allele. In control experiments conducted prior to the screen, we found that br^1 animals (hemizygous males and homozygous br^1 females), maintained at 21°, display malformed legs at a low frequency of 0.4% ($n = 3629$). For the purpose of this screen, we arbitrarily considered an interaction to be significant if 20% or more of the $br^1/Y;Df/+$ animals displayed at least one malformed second or third leg, representing a 50-fold increase over the br^1 background.

Out of an initial collection of 154 autosomal deficiency stocks, we tested 133 stocks for genetic interactions with br^1. The remaining deficiency stocks could not be tested either because of unmarked duplications that prevented unambiguous identification of progeny classes or due to the presence of *Sb/sbd* alleles on the deficiency chromosome that would obscure a possible genetic interaction with br^1 (Beaton *et al.* 1988). Of the 133 deficiency stocks screened, 43 reproducibly enhance the malformed leg phenotype associated with br^1 (Figure 1, open boxes). To confirm these interactions and refine the genomic regions containing the putative br^1-interacting loci, we tested >175 additional deficiency stocks that were predicted to overlap with br^1-interacting deficiency stocks identified in the primary screen. Overall, we found 64 deficiency stocks that enhance the br^1 leg phenotype to >20% (Table 1). We also tested >425 *P*-element-insertion stocks and individual mutations in candidate genes in an attempt to identify single loci that could account for the br^1 interaction detected with the deficiency stocks. From these studies we found 17 br^1-interacting loci and identified mutations in three genes that act as dominant enhancers of the malformed leg phenotype of br^1.

***Rho1*:** Five overlapping deficiency stocks, *Df(2R)Jp1*, *Df(2R)Jp4*, *Df(2R)Jp5*, *Df(2R)Jp7*, and *Df(2R)Jp8*, enhance the br^1 malformed leg phenotype to frequencies ranging from 23 to 78% (Table 1). Each of these deficiencies is predicted to remove sequences in the 52F cytological region. We tested five *P*-element-insertion stocks from this interval and found one, *l(2)k02107*, that also strongly enhances br^1 (Table 2). Plasmid rescue of genomic DNA adjacent to the *P*-element-insertion site revealed that *l(2)k02107* is an insertion into an intron of the *Rho1* gene, confirming a subsequent report that this *P*-element mutation is a *bona fide* allele of *Rho1* (Magie *et al.* 1999). To verify the dominant genetic interaction between *Rho1* and br^1, we tested $Rho1^{l3.8}$ and $Rho1^{E3.10}$ and found that both alleles also strongly enhance the malformed leg phenotype of br^1 (Table 2). Interestingly, Halsell *et al.* (2000) found that whereas *Rho1* fails to complement *Df(2R)Jp4* and *Df(2R)Jp8*, it fully complements *Df(2R)Jp1*. Our finding of a strong dominant genetic interaction between br^1 and *Df(2R)Jp1* therefore suggests the presence of another br^1-interacting locus in the cytogenetic interval 51D3-52F9. A potential candidate gene mapping to this region is *myosin light chain kinase*. A direct test of this candidate, however, awaits the identification of a specific mutation in this gene.

***blistered*:** *Df(2R)Px2* (60C05;60D09-10) is a very strong dominant enhancer of the br^1 malformed leg phenotype, producing malformed legs at a frequency of 50% (Table 1). Crosses with an overlapping deficiency, *Df(2R)Px1* (60B08-10;60D01-02), produced malformed legs at a frequency of 19% ($n = 112$) in the br^1 genetic background, mapping the br^1-interacting locus to the 60C5-D1 interval. Mutations in *blistered* (*bs*), which encodes the Drosophila SRF transcription factor, fail to complement these two deficiencies, and bs^2 was previously shown to enhance the malformed leg phenotype of br^1, suggesting that *bs* might contribute to the interaction seen with these deficiencies (Gotwals and Fristrom 1991; Affolter *et al.* 1994). To confirm these results, we tested three alleles of *bs* for a dominant genetic interaction with br^1 and found that bs^{k03267}, a *P*-element-insertion allele, displays a frequency of 15% malformed legs, whereas the *P*-element-insertion allele bs^{k03267} displays a weaker interaction of 9% (Table 2). The genetic interactions with both alleles are cold sensitive, showing a dramatic increase in the percentage of animals displaying malformed legs at 18° (Table 2). bs^{ha} fails to interact with br^1 at either temperature (Table 2). The allele specificity and cold sensitivity of these genetic interactions are consistent with earlier observations (Gotwals and Fristrom 1991). We conclude that *bs* is a dominant enhancer of br^1 and that its absence in *Df(2R)Px2* contributes to the genetic interaction we observe between this deficiency and br^1.

***cytoskeletal Tropomyosin*:** *Df(3R)ea* (88E07-13;89A01) enhances the malformed leg phenotype of br^1 with a frequency of 62% (Table 2), a particularly strong enhancement. We were unable to refine the interval containing the br^1-interacting locus using available deficiencies and therefore tested 20 *P*-element-insertion stocks that map within the interval from 88E1 to 89A9. We found one stock, *l(3)2299*, that acts as a dominant enhancer of br^1 and also fails to complement *Df(3R)ea* (Table 2; Tetzlaff *et al.* 1996). *l(3)2299* results from a *P*-element insertion into the twentieth codon of a cytoskeletal-specific exon of *Tm1* (Tetzlaff *et al.* 1996). To confirm this interaction, we tested a maternal-effect

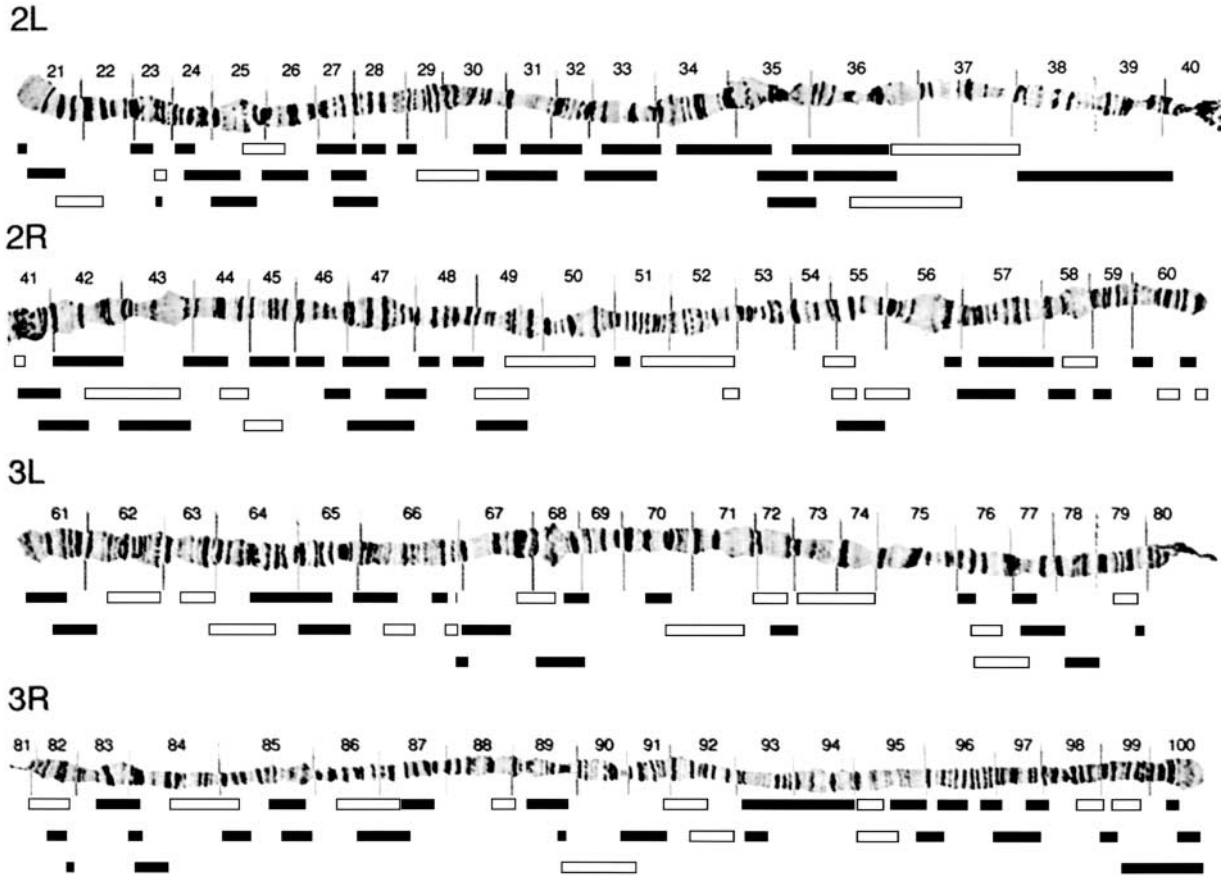

FIGURE 1.—Chromosomal deficiencies that enhance the *br*[1] malformed leg phenotype. Shown are 133 deficiencies from the primary screen that were tested for dominant enhancement of the *br*[1] malformed leg phenotype. Open boxes indicate the chromosomal extent of deficiencies that show >20% malformed legs when heterozygous in a *br*[1] background (*br*[1]*/Y;Df/+*). Noninteracting deficiencies are represented by solid boxes. Polytene chromosome images are from LEFEVRE (1976).

mutation in *cytoskeletal Tropomyosin* (*cTm*; *Tm1*[eg9]; ERDELYI *et al.* 1995) and found that it weakly enhances *br*[1] (Table 2), although a lethal excision allele generated from this mutation, *cTm*[er4] (ERDELYI *et al.* 1995), does not enhance the *br*[1] malformed leg phenotype (Table 2). In Drosophila there are two tandem *tropomyosin* genes (*Tm1* and *Tm2*) that produce several muscle-specific isoforms and one cytoskeletal-specific isoform due to alternative splicing. We therefore tested a hypomorphic allele of *Tm2* that specifically affects jump and indirect flight muscles and found that it does not act as a dominant enhancer of the malformed leg phenotype of *br*[1] (Table 2). We conclude that *br*[1] interacts with *cTm* (*Tm1*) and that this interaction contributes to the observed dominant enhancement of *br*[1] by *Df(3R)ea*.

Other interacting loci defined by deficiencies: In addition to the genetic interactions of *br*[1] with *Rho1*, *bs*, and *cTm*, we predict that at least seven loci on the second chromosome and at least seven loci on the third chromosome harbor *br*[1]-interacting genes (Table 1). This prediction is based on the finding of two or more overlapping *br*[1]-interacting deficiency stocks that were derived from different parental chromosomes (Table 1). In five cases, each of the overlapping deficiency stocks produce an interaction phenotype at a frequency of >40%, >100-fold over the *br*[1] background. Of these, one interval is particularly noteworthy. *Df(3R)D6*, *Df(3R)D7*, and *Df(3R)p712* compose a set of three overlapping deficiencies that remove genomic sequences from 84D04 to 84F02. Efforts to identify a *br*[1]-interacting gene within this interval have thus far failed, although we have tested 36 deficiency stocks, 16 *P*-element-insertion stocks, and 21 representative EMS alleles derived from a saturation mutagenesis screen of this region (BAKER *et al.* 1991). Of the remaining candidate genes within this interval, one gene in particular stands out, *ImpE3*. This gene was originally isolated in a molecular screen for genes that encode ecdysone-inducible cell-surface or secreted imaginal disc proteins (NATZLE *et al.* 1986). Subsequent experiments confirmed that *ImpE3* is induced by ecdysone and strongly expressed in imaginal discs (MOORE *et al.* 1990). At present there are no mutant alleles of *ImpE3* to test for a genetic interaction with *br*[1], but Northern blot analysis of *ImpE3* expression in *br* mutant imaginal discs has demonstrated a regulatory interaction between these two genes (see below).

TABLE 1

Summary of *br*^{1}-interacting deficiencies

Deficiency stock	Deficiency breakpoints	*br*^{1}*/Y;Df/+*: % malformed (*n*)[a]	Comments[b]
Df(2L)ast2	021D01-02;022B02-03	29 (350)	
In(2LR)DTD16^{L}*DTD42*^{R}*, bw*^{1} *sp*^{1}	023C;023E03-06	38 (302)	
Df(2L)cl-h3	025D02-04;026B02-05	53 (191)	Interval 26A-B
In(2LR)DTD116^{L}*DTD24*^{R}*, (net*^{1}*) bw*^{1} *sp*^{1}	026A04-06;026C01-02	30 (223)	Interval 26A-B
Df(2L)N22-14	029C01-02;030C08-09	48 (238)	
Df(2L)VA18, m^{1} *pr*^{1}	036C04-D01;036F	25 (115)	Interval 36E-F
Df(2L)TW50, cn^{1}	036E04-F01;038A06-07	61 (241)	Interval 36E-F
Df(2L)TW3, l(2)74i^{1}	036F07-09;037B02-07	23 (70)	Interval 36E-F
Df(2L)pr-A16, cn^{1} *bw*^{1}	037B02-12;038D02-05	46 (105)	Interval 37B-D
Df(2L)VA12, cn^{1} *bw*^{1}	037C02-05;038B02-C01	36 (147)	Interval 37B-D
Df(2L)pr-A14, cn^{1} *bw*^{1}	037D02-07;039A04-07	31 (87)	Interval 37B-D
Df(2R)M41A4	41A (within)	64 (149)	
Df(2R)ST1, Adh^{n5} *pr*^{1} *cn**	042B03-05;043E15-18	29 (363)	
Df(2R)Np3, bw^{1}	044D02-E01;045B08-C01	81 (37)	Interval 44D-F
Df(2R)H3E1	044D01-04;044F12	40 (217)	Interval 44D-F
Df(2R)Np5, In(2LR)w45-32n, cn^{1}	044F10;045D09-E01	60 (196)	Interval 44D-F
Df(2R)Np4, bw^{1}	044F11;045C01	70 (103)	Interval 44D-F
Df(2R)vg-C	049A04-13;049E07-F01	32 (309)	Interval 49C-F
Df(2R)CX1, b^{1} *pr*^{1}	049C01-04;050C23-D02	20 (109)	Interval 49C-F
Df(2R)Jp1	051D03-08;052F05-09	45 (322)	Interval 51D-52F (*mlck?*)
Df(2R)Jp4	051F13;052F08-09	52 (90)	Interval 51D-52F (*mlck?*)
Df(2R)Jp5	052A13-B03;052F10-11	78 (49)	Interval 51D-52F (*mlck?*); *Rho1*
Df(2R)Jp7, w^{+}	052F05-09;052F10-11	23 (189)	*Rho1*
Df(2R)Jp8, w^{+}	052F05-09;052F10-53A01	26 (384)	*Rho1*
Df(2R)Pcl7B	054E08-F01;055B09-C01	28 (120)	Interval 54E-55B
Df(2R)RM2-1	054F02;056A01	80 (74)	Interval 54E-55B
Df(2R)Pcl11B, al^{1} *dp*^{ov1} *b*^{1} *pr*^{1}	054F06-55A01;055C01-03	26 (285)	Interval 54E-55B
Df(2R)P34	055E02-04;056C01-11	25 (289)	
Df(2R)X58-8, pr^{1} *cn*^{1}	058B03;059A01	49 (68)	
Df(2R)X58-12	058D01-02;059A	42 (337)	
Df(2R)Px2	060C05-06;060D09-10	50 (264)	*bs*
Df(2R)Kr10, b^{1} *pr*^{1} *Bl*^{1} *c*^{1}	060F01;060F05	20 (219)	
Df(3L)R-G7, rho$^{ve\text{-}1}$	062B08-09;062F02-05	22 (228)	
Df(3L)HR218, Dp(3;3)pdp7, ca^{1}	063A02-07;063B09-10	34 (398)	
Df(3L)HR119	063C02;063F07	31 (212)	Interval 63F
Df(3L)GN24	063F06-07;064C13-15	28 (160)	Interval 63F
Df(3L)66C-G28	066B08-09;066C09-10	32 (349)	
Df(3L)Scf-R6, th^{1} *st*^{1} *cu*^{1} *sr*^{1} *e*^{s} *ca*^{1}	066E01-06;066F01-06	30 (251)	
Df(3L)lxd6	067E05-07;068C02-04	27 (332)	
Df(3L)fz-M21, st^{1}	070D02-03;071E04-05	45 (210)	
Df(3L)Brd6, p^{b}	070E;071F	31 (131)	Interval 71F
Df(3L)brm11	071F01-04;072D01-10	30 (315)	Interval 71F
Df(3L)81k19	073A03;074F	23 (217)	
Df(3L)XS2182	076B;076F	82 (118)	Interval 76B-D
Df(3L)XS543	076B;077A	63 (134)	Interval 76B-D
Df(3L)kto2	076B01-02;076D05	46 (187)	Interval 76B-D
Df(3L)XS533	076B04;077B	59 (243)	Interval 76B-D
Df(3L)XS572	076B06;077C01	37 (49)	Interval 76B-D
Df(3L)Ten-m-AL29	079C01-03;079E03-08	20 (230)	
Df(3R)ME15, mwh^{1} *red*^{1} *e*^{4}	081F03-06;082F05-07	21 (260)	
Df(3R)D6, Ubx^{1} *e*^{4}	084D02-03;084F13-16	89 (37)	Interval 84D-F (*ImpE3?*)
Df(3R)D7, Ubx^{1} *e*^{4}	084D03-05;084F01-02	75 (235)	Interval 84D-F (*ImpE3?*)
Df(3R)p712, red^{1} *e*^{1}	084D04-06;085B06	51 (169)	Interval 84D-F (*ImpE3?*)
Df(3R)p25, Df(3R)P2	085A03;085B01, 089D09-E01;089E02-03	53 (100)	Interval 89E-90D?
Df(3R)M-Kx1	086C01;087B01-05	43 (153)	
Df(3R)ea, kni$^{ri\text{-}1}$ *p*^{b}	088E07-13;089A01	62 (436)	*cTm*
Df(3R)DG2	089E01-F04;091B01-B02	60 (111)	Interval 89E-90D; SSNC of *br*^{5}

(*continued*)

TABLE 1

(Continued)

Deficiency stock	Deficiency breakpoints	$br^1/Y;Df/+$: % malformed (n)[a]	Comments[b]
Df(3R)RD31	089E02;090D	54 (117)	Interval 89E-90D
Df(3R)Dl-BX12, ss^1 e^4 ro^1	091F01-02;092D03-06	51 (186)	Interval 92B-D
*Df(3R)H-B79, e**	092B03;092F13	48 (60)	Interval 92B-D
Df(3R)mbc-30	095A05-07;095C10-11	32 (286)	Interval 95A-C
Df(3R)mbc-R1, ry506	095A05-07;095D06-11	39 (366)	Interval 95A-C
Df(3R)3450	098E03;099A06-08	27 (225)	
Df(3R)L127	099B05-06;099E04-F01	36 (14)	

[a] % malformed indicates the percentage of $br^1/Y;Df/+$ animals showing the malformed leg phenotype in at least one leg. n, total number of flies of the indicated genotype that were scored.

[b] Interval listings indicate br^1-interacting loci defined by two or more overlapping deficiencies derived from different parental chromosomes each showing >20% malformed legs. br^1-Interacting genes that fail to complement the indicated deficiencies are underlined. Genes followed by ? symbol are possible candidates discussed in text.

***br^5* second-site noncomplementation screen with deficiency stocks:** We conducted SSNC tests between a collection of 133 autosomal deficiency stocks and br^5, an amorphic allele of *br*, to determine whether a stronger allele might identify novel *br*-interacting genes. In pilot studies we were unable to detect malformed legs in $br^5/+$ females and therefore set an arbitrary threshold for significant interaction at 5% malformed legs in the $br^5/+;Df/+$ genotypic class. Surprisingly, we found only one deficiency that specifically and reproducibly interacts with br^5 in this SSNC assay. *Df(3R)DG2* (89E01-F04;92D03-06) displays malformed legs at a frequency of 11% (n = 62) when heterozygous in a $br^5/+$ genetic background. *Df(3R)DG2* also shows a very strong dominant genetic interaction with br^1 (Table 1).

***br^1* dominant genetic interaction screen of EMS-treated animals:** There are two significant limitations when chromosomal deficiencies are used for a genetic interaction screen: incomplete coverage of the genome and the requirement for detecting an interaction with an amorphic allele. In an effort to overcome these limitations, we conducted an F_1 screen of EMS-treated animals. We mutagenized br^1 males, mated them to br^1 virgin females, and screened through ~112,000 F_1 progeny for flies displaying the malformed leg phenotype. Malformed progeny were backcrossed to br^1 animals to generate stocks. These stocks were then maintained for several generations as *inter se* crosses, selecting for animals with malformed legs to remove unlinked second-site mutations by free recombination. We kept those stocks in which the *inter se* crosses produced ~10% or more malformed progeny at the F_5 generation. From this screen we identified 26 mutations that map to a single chromosome and reproducibly enhance the br^1 leg phenotype. Two *E(br)* mutations map to the X chromosome, 9 map to the second chromosome, and 15 map to the third chromosome. We have analyzed 20 of these *E(br)* lines in detail (Tables 3 and 4). Lethal complementation analyses revealed one complementation group consisting of six members that maps to the third chromosome, one complementation group with two members that maps to the second chromosome, and 12 *E(br)* mutations that complement every other *E(br)* mutation. Six of these map to the second chromosome and 6 map to the third chromosome.

Complementation analyses identify *Rho1*, *sbd*, and *bs* alleles as *E(br)* mutations: As a first step toward identi-

TABLE 2

***br^1*-Interacting genes identified through deficiency screens**

Deficiency stock or allele[a]	Cytology[b]	$br^1/Y;*/+$: % malformed (n)[c]
Df(2R)Jp5	052A13-B03;052F10-11	78 (49)
Df(2R)Jp7	052F05-09;052F10-11	23 (189)
Df(2R)Jp8	052F05-09;052F10-53A01	26 (384)
Rho1^{k02107}	052F08-09	79 (106)
Rho1$^{E3.10}$	052F08-09	62 (53)
Rho1$^{J3.8}$	052F08-09	27 (78)
Df(2R)Px1	060B08-10;60D01-02	19 (112)
Df(2R)Px2	060C05;60D09-10	50 (264)
bs^{k03267}	060C06-07	15 (157)
bs^{k07909}	060C06-07	9 (281)
bs^{ba}	060C06-07	3 (183)
bs^{k03267} @18°	060C06-07	73 (300)
bs^{k07909} @18°	060C06-07	30 (103)
bs^{ba} @18°	060C06-07	3 (59)
Df(3R)ea	088E07-13;089A01	62 (436)
Tm1^{2299}	088E12-13	27 (172)
Tm1^{rg9}	088E12-13	14 (44)
Tm1^{er4}	088E12-13	4 (150)
Tm2^3	088E12-13	2 (254)

[a] All crosses were maintained at 21°, except where indicated.

[b] Deficiency breakpoints and cytological location of *bs* and *Tm1* are taken from FlyBase (1999); cytological location of *Rho1* was determined by Halsell *et al.* (2000).

[c] % malformed indicates the percentage of animals of the indicated genotype showing the malformed leg phenotype in at least one leg. n, total number of flies of the indicated genotype that were scored.

TABLE 3

Summary of F_1 second-site modifier screen

Complementation group	Chromosomal location[a]	Malformed leg phenotype[b]	% malformed (n)[c]		
			w^{1118};*E(br)*/+	*br*^{1};*E(br)*/+	*br*^{5}/*w*;*E(br)*/+
sbd$^{E(br)20}$	89B	Fe	0 (101)	28 (80)	2 (60)
sbd$^{E(br)48}$	89B	Fe	0 (133)	19 (63)	7 (59)
sbd$^{E(br)228}$	89B	Fe	0 (46)	5 (116)	0 (52)
sbd$^{E(br)448}$	89B	Fe	0 (171)	38 (105)	25 (48)
sbd$^{E(br)536}$	89B	Fe	0 (126)	17 (59)	2 (51)
sbd$^{E(br)623}$	89B	Fe	1 (217)	19 (47)	0 (49)
Rho1$^{E(br)233}$	52F8-9	Fe	1 (104)	21 (38)	8 (49)
Rho1$^{E(br)246}$	52F8-9	Fe	3 (127)	18 (57)	9 (33)
bs$^{E(br)292}$	60C6-7	Fe	0 (120)	15 (65)	10 (51)
E(br)24	2-[58-59]	Ti	9 (134)	30 (99)	0 (46)
E(br)65	2-[22-31]	Fe	2 (125)	45 (20)	17 (36)
E(br)155	2-[35-38]	Ta	7 (121)	29 (52)	7 (57)
E(br)165	2-[17-31]	Ta	1 (75)	100 (55)	2 (53)
E(br)333	Chromosome 2	Ti	5 (230)	29 (76)	19 (27)
E(br)72	Chromosome 3	Fe	0 (105)	7 (173)	0 (70)
E(br)121	3-[41-43] 70C-E	Ti	12 (206)	92 (62)	53 (62)
E(br)160	Chromosome 3	Fe	2 (157)	10 (113)	3 (59)
E(br)187	Chromosome 3	Fe	1 (88)	53 (34)	0 (54)
E(br)420	3-[60-61] 89E-90D	Ti, Ta (first leg)	2 (64)	24 (46)	4 (55)
E(br)444	Chromosome 3	Ti	9 (306)	27 (85)	5 (38)

[a] Chromosomal locations for *Sb/sbd* and *bs* are derived from FlyBase (1999). Cytological location of *Rho1* was determined by Halsell *et al.* (2000). Meiotic mapping results are indicated in brackets. Cytogenetic designations are based upon noncomplementing deficiencies.

[b] Predominant malformed leg phenotype observed in *br*^{1}*/Y;E(br)/+* animals: Fe, short, fat femurs and tibias (see Figure 3B); Ta, short, fat tarsal segments with normal femurs and tibias (see Figure 3C); Ti, moderate-to-strong bend in mid-tibia not associated with ectopic joint (see Figure 3D); Ti, Ta (first leg), short thin tibias and tarsal segments, sometimes missing these elements, predominantly in the first leg.

[c] % malformed indicates the percentage of animals of the indicated genotype showing the malformed leg phenotype in at least one leg. *n*, total number of flies of the indicated genotype that were scored.

fying the *br*^{1}-interacting genes disrupted by the EMS mutations, we performed a large-scale complementation analysis between each of the *E(br)* lines and a panel of deficiencies and specific mutations. This set of stocks included representative *br*^{1}-interacting deficiencies from each of the intervals identified in the deficiency screen, as well as mutations in *bs*, *Rho1*, *RhoGEF2*, *sbd*, *cTm*, and *zip*. From these analyses we determined that the large complementation group on the third chromosome is allelic to *Sb/sbd* on the basis of the following four observations. First, *E(br)20*, *E(br)48*, *E(br)448*, *E(br)536*, and *E(br)623* compose a single complementation group, and *E(br)228* partially fails to complement these mutations for lethality. Second, *E(br)20*, *E(br)536*, and *E(br)623* fail to complement *sbd*^{45}. Third, complementation tests between these same three *E(br)* lines and *sbd*^{105} produce viable *trans*-heterozygous adults that show a stubble bristle phenotype. Fourth, *E(br)228* is partially viable, producing homozygous mutant adults at ~20% of the expected frequency, all of which show a completely penetrant stubble bristle phenotype (Figure 2B). All of the *sbd*$^{E(br)}$ mutations show normal bristle morphology when heterozygous, classifying all six alleles as *sbd* with respect to the bristle phenotype (Figure 2A). Similar complementation analyses demonstrated that *E(br)233* and *E(br)246* are allelic to *Rho1*. Both mutations fail to complement one another, *E(br)246* fails to complement *Df(2R)Jp8* (52F05-09; 52F10-53A01), and both mutations fail to complement *Rho1*^{k02107}, *Rho1*$^{l3.8}$, and *Rho1*$^{E3.10}$. Finally, *E(br)292* is allelic to *bs* on the basis of its failure to complement *Df(2R)Px2* (60C05;60D09-10) and two *bs* alleles, *bs*^{k03267} and *bs*^{k07909}.

Meiotic mapping of the *E(br)* mutations: Our complementation studies revealed one instance of noncomplementation between an *E(br)* mutation and a *br*^{1}-interacting deficiency. *E(br)420* fails to complement *Df(3R)RD31* (89E02;90D) and *Df(3R)DG2* (89E01-F04;91B01-02). It does, however, fully complement *Df(3R)C4* (89E03-04;90A01-07), suggesting that the *E(br)420* mutation is located in 89E02-04 or 90A-D. To verify this mapping, we performed meiotic mapping experiments with *br*^{1}*;ru th st ri roe p e ca*. We conducted these crosses in the *br*^{1} genetic background to specifically map the *br*^{1}-interacting mutation rather than a lethal lesion that might be linked but not causative of the interaction (see materials and methods). Recombination distance from *thread* (3-[43.2] on the recombination map) places *E(br)*

TABLE 4

Lethal-phase and terminal phenotypic analyses of *E(br)* mutations

Complementation group	Embryonic lethality[a]	Larval lethality[b]	Phenotype[c]
$sbd^{E(br)20}$	10 ± 3	100	Molt
$sbd^{E(br)48}$	13 ± 2	91 ± 5	Molt, AO
$sbd^{E(br)228}$	7 ± 3	34 ± 10	Molt
$sbd^{E(br)448}$	17 ± 10	100	Molt
$sbd^{E(br)536}$	14 ± 6	97 ± 3	Molt
$sbd^{E(br)623}$	15 ± 3	85 ± 4	Molt, AO
$Rho1^{E(br)233}$	100	NA	AO, GBR
$Rho1^{E(br)246}$	100	NA	AO, GBR
$bs^{E(br)292}$	18 ± 3	53 ± 7	AO, Tr, Ba
E(br)24	25 ± 7	34 ± 7	AO
E(br)65	14 ± 9	100	AO
E(br)155	97 ± 1	ND	DO, AO
E(br)165	100	NA	DO, naked
E(br)333	44 ± 7	97 ± 1	NP
E(br)72	98 ± 2	ND	NP
E(br)121	99 ± 1	ND	NP
E(br)160	6 ± 2	25 ± 3	NP
E(br)187	8 ± 4	49 ± 4	NP
E(br)420	3 ± 1	99 ± 1	NP
E(br)444	21 ± 2	100	NP

[a] Mean ± SE of embryonic lethality from three independent experiments.

[b] Mean ± SE of larval lethality from three independent experiments. Mutant larvae were picked as newly hatched first instar larvae. NA, not applicable; ND, not determined.

[c] Phenotype of *w; E(br)* homozygous animals: Molt, larval molting defects; AO, anterior open embryonic cuticle; GBR, germband retraction incomplete; DO, dorsal open embryonic cuticle; Tr, terminal branching of the larval tracheae missing; Ba, failure of apposition of the dorsal and ventral wing surfaces that give rise to tube- or balloon-shaped wing. NP, no discernible embryonic phenotype.

420 at 59.9 on the recombination map, which approximately corresponds to 89F (FlyBase 1999). Similarly, recombination distance from *scarlet* (3-[44]) places *E(br)420* at 60.7 and from *radius incompletus* (3-[46.8]) at 60.8 on the recombination map, both of which correspond roughly to 90D. The meiotic mapping data therefore support the complementation data and place *E(br)420* in 89E02-04 or 90A-D (Table 3).

In addition to *E(br)420*, we used meiotic mapping to locate the br^1-interacting mutations in *E(br)24*, *E(br)65*, *E(br)121*, *E(br)155*, and *E(br)165* (Table 3). The mapping of *E(br)121* to 3-[41-43] (corresponding to 70C-71C) is supported by the failure of *E(br)121* to complement *Df(3L)fz-CALS* (70C02-06;70E01). We are currently attempting to confirm the meiotic mapping of the other four *E(br)* mutations through complementation studies and are beginning the initial mapping of the remaining five *E(br)* mutations.

Characterization of the *E(br)* mutations: We undertook preliminary characterization of the *E(br)* mutations as a first step toward understanding the function of the affected genes. To this end we have: (1) determined the penetrance of the dominant genetic interaction with br^1 (Table 3), (2) tested for SSNC with an amorphic allele of *br* (Table 3), (3) conducted thorough lethal-phase and terminal phenotypic analyses of the *E(br)* mutations (Table 4), (4) conducted SSNC analyses with representative mutations in the Rho1 pathway (Table 5), and (5) performed Northern blot analysis of br^1-interacting genes on RNA collected from staged wild-type and br^5 mutant imaginal discs (Figure 5). The results of these studies are reported below.

Phenotypic analyses of interactions between br^1 and the *E(br)* mutations: Individual *E(br)* mutations vary in their ability to enhance the br^1 malformed leg phenotype, ranging from 5% for $sbd^{E(br)228}$ to 100% for *E(br)165* (Table 3). Eight *E(br)* mutations enhance br^1 with a penetrance of <20%, which is the threshold used for the deficiency screen. These results are, however, significant because the *E(br)* mutations were generated in a uniform genetic background, unlike the wide range of genetic backgrounds found in the deficiency stocks. Therefore, for example, the 5% malformations seen in br^1/Y; $sbd^{E(br)228}/+$ animals represent a 12-fold increase over br^1/Y that can be attributed primarily to the mutation. It is also noteworthy that the poorest interacting mutation is an allele of *Sb/sbd*, a known br^1-interacting gene (Beaton *et al.* 1988).

The malformed leg phenotypes in br^1/Y;*E(br)*/+ males can be classified into three distinct classes, as shown in Figure 3. Fourteen of the *E(br)* mutant lines produce legs that have short, fat femurs and tibias that are often kinked or twisted (Figure 3B; Table 3). Included in this group of mutations are all the *sbd*, *Rho1*, and *bs* alleles. In two *E(br)* lines, the interaction phenotype is predominantly restricted to the tarsal segments, which are shorter and fatter than those of wild type (Figure 3C; Table 3). In four *E(br)* lines, the interaction phenotype consists entirely of a moderate to strong bend in the mid-tibia that is not associated with an ectopic joint (Figure 3D; Table 3). In all cases, the defects manifest themselves in the third pair of legs and are often unilateral. Malformations of the second pair of legs occur much less frequently and are almost always associated with extreme malformations of the third pair of legs. *E(br)420* is unique in producing malformations at a high frequency in the first pair of legs. In this case, the malformed legs show defects primarily in the tibia and tarsal segments, and occasionally the first pair legs are missing middle tarsal segments (data not shown). We have not, however, quantified these phenotypes. Finally, we occasionally observe wing malformations as a br^1 interaction phenotype with the *E(br)* mutations. We did not quantify these phenotypes because their penetrance is low and the expressivity is more varied than that of the malformed leg phenotypes.

We also outcrossed the br^1 allele and examined

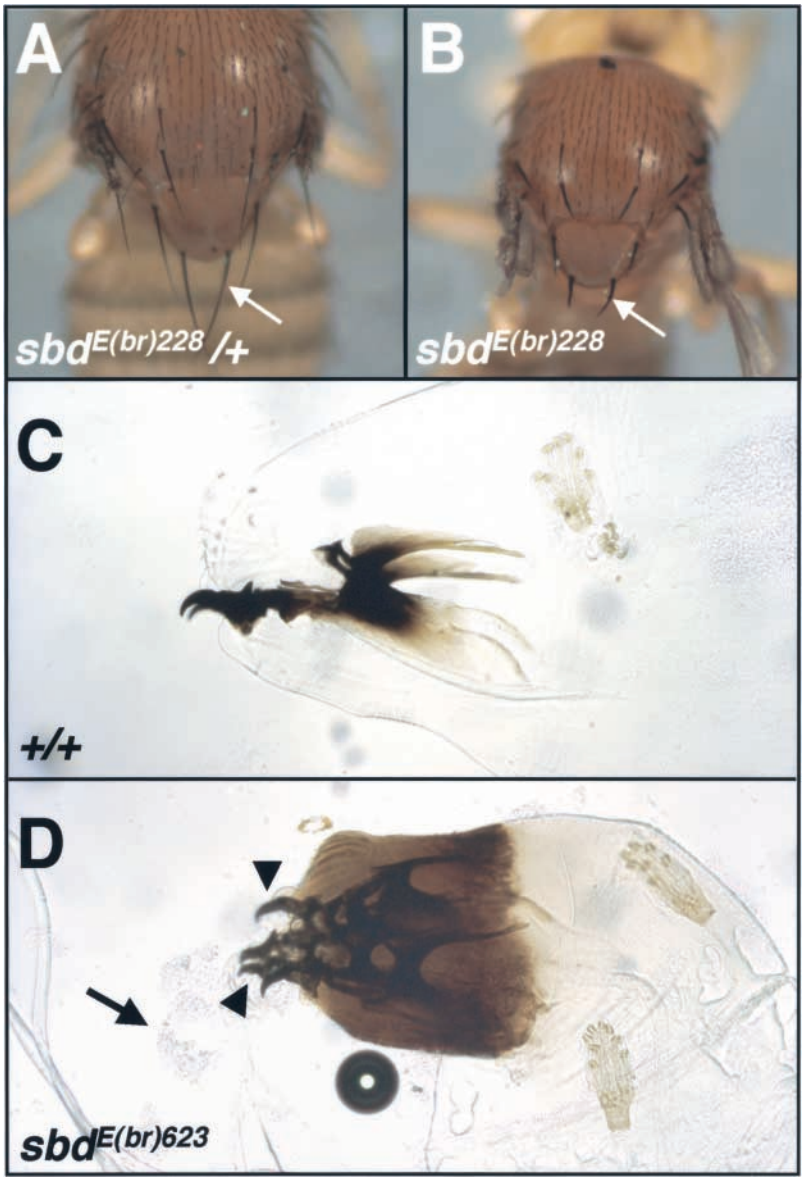

Figure 2.—The bristle phenotype and molting defects associated with *sbd* mutations. Brightfield photomicrographs are shown of (A) the dorsal thorax from an $sbd^{E(br)228}$/+ heterozygous adult and (B) an $sbd^{E(br)228}$ homozygous adult. Note the short, thick, and barb-ended scutellar bristles on the $sbd^{E(br)228}$ thorax relative to the long and thin wild-type bristles on the $sbd^{E(br)228}$/+ thorax (arrows). Depicted below are brightfield photomicrographs of cuticle preparations showing the anterior regions of (C) wild-type and (D) $sbd^{E(br)623}$ mutant third instar larvae. The mutant larva has retained an extra set of mouth hooks and head skeleton (arrowheads) along with some attached cuticle from the previous molt (arrow). $sbd^{E(br)623}$ mutants also show an unusual sclerotization of the anterior epidermis.

w^{1118};*E(br)*/+ animals for the presence of malformed legs. This study revealed that five of the *E(br)* mutations show a semidominant malformed leg phenotype. *E(br)24*, *E(br)121*, *E(br)155*, *E(br)333*, and *E(br)444* all show >5% malformed legs under these conditions (Table 3). In each case, however, the penetrance of malformed legs in the br^1 background is at least threefold higher. Interestingly, all four of the *E(br)* mutant lines that show the bent tibia malformed leg phenotype are also semidominant (Figure 3D; Table 3).

SSNC analyses between *E(br)* mutations and br^5: To test the specificity of the *E(br)* mutations we conducted SSNC experiments with br^5. Whereas only one deficiency from the deficiency screen showed >5% malformed legs in this assay (see above), 10 of the *E(br)* mutations display >5% malformed legs when heterozygous in a br^5/w^{1118} genetic background (Table 3). Included in this collection are two *sbd* alleles, both *Rho1* alleles, the *bs* allele and five of the unidentified *E(br)* mutations. The percentage of malformed legs seen with *E(br)155* and *E(br)444* in a br^5/w^{1118} genetic background, however, was similar to the level of malformed legs found in w^{1118}; *E(br)*/+ animals, arguing against a relevant genetic interaction.

Lethal-phase and terminal phenotypic analyses of *E(br)* mutants: To characterize the function of the genes disrupted by the *E(br)* mutations, we conducted lethal-phase studies using balancer chromosomes that express GFP to unambiguously identify homozygous mutant embryos and larvae (Table 4). These experiments revealed that both $Rho1^{E(br)233}$ and $Rho1^{E(br)246}$ show completely penetrant embryonic lethality with nearly every embryo possessing a large dorsal anterior hole with the head skeleton extruded (Figure 4, B and C). In addition, 5–10% of these embryos possess a second cuticular hole often positioned near the posterior pole (data not shown),

TABLE 5

Second-site noncomplementation analyses with Rho1 pathway mutations

Complementation group	$Rho1^{J3.8}$	$Rho1^{k02107}$	$Rho1^{E3.10}$	$RhoGEF2^{04291}$	$RhoGEF2^{11-3}$	$zip^{E(br)}$	zip^{1}	zip^{33-1}
$sbd^{E(br)20}$	16 (45)	8 (67)	11 (72)	1 (116)	3 (100)	46 (90)	0 (80)	0 (92)
$sbd^{E(br)48}$	15 (61)	2 (99)	8 (76)	2 (109)	3 (63)	30 (79)	0 (120)	2 (104)
$sbd^{E(br)228}$	3 (61)	12 (61)	2 (85)	4 (102)	2 (86)	14 (52)	0 (109)	0 (109)
$sbd^{E(br)448}$	15 (48)	2 (50)	9 (90)	4 (91)	4 (122)	57 (53)	1 (113)	11 (228)
$sbd^{E(br)536}$	19 (57)	10 (58)	14 (72)	2 (111)	2 (119)	33 (73)	0 (118)	2 (112)
$sbd^{E(br)623}$	21 (38)	2 (58)	2 (116)	0 (100)	0 (109)	26 (73)	0 (135)	0 (108)
$Rho1^{E(br)233}$	NA	NA	NA	4 (95)	62 (71)	93 (28)	2 (116)	81 (128)
$Rho1^{E(br)246}$	NA	NA	NA	17 (69)	63 (49)	83 (41)	6 (65)	90 (114)
$bs^{E(br)292}$	7 (76)	0 (89)	0 (77)	0 (112)	0 (141)	2 (98)	0 (73)	0 (100)
E(br)24	11 (95)	3 (37)	23 (83)	2 (130)	5 (130)	9 (96)	11 (110)	11 (161)
E(br)65	28 (87)	6 (48)	16 (116)	4 (100)	28 (109)	67 (36)	2 (131)	7 (162)
E(br)155	57 (79)	0 (73)	16 (103)	6 (78)	1 (114)	7 (89)	1 (193)	4 (97)
E(br)165	15 (73)	7 (58)	10 (88)	7 (179)	1 (85)	6 (79)	6 (64)	1 (113)
E(br)333	1 (76)	6 (63)	5 (58)	9 (67)	3 (108)	4 (47)	3 (61)	1 (98)
E(br)72	16 (50)	5 (74)	6 (64)	1 (138)	3 (107)	4 (107)	1 (134)	0 (110)
E(br)121	37 (57)	56 (52)	37 (62)	49 (53)	0 (88)	82 (66)	32 (72)	1 (91)
E(br)160	7 (58)	8 (78)	4 (93)	2 (116)	4 (99)	20 (77)	1 (99)	2 (109)
E(br)187	1 (88)	2 (41)	0 (98)	2 (125)	1 (90)	6 (91)	0 (106)	1 (104)
E(br)420	21 (47)	2 (56)	1 (76)	3 (119)	6 (88)	15 (61)	2 (50)	3 (118)
E(br)444	29 (38)	37 (27)	6 (133)	36 (120)	44 (93)	84 (73)	1 (158)	4 (83)

The value outside the parentheses indicates the percentage of animals doubly heterozygous for the indicated mutations showing the malformed leg phenotype in at least one leg. The value inside the parentheses indicates the total number of flies doubly heterozygous for the indicated mutations that were scored. SSNC interactions producing ≥20% malformations are underlined.

and many of the dead embryos display slight curvature of the ventral surface, indicating a mild defect in germband retraction (Figure 4C). These observations are consistent with phenotypic analyses describing the zygotic loss-of-function phenotypes for *Rho1* mutations (Magie *et al.* 1999) and suggest that both of these new *Rho1* mutations are strong loss-of-function alleles.

Lethal-phase analysis of $bs^{E(br)292}$ indicated a requirement for *bs* throughout the life cycle (Table 4). The predominant lethal period occurs during larval stages, although we also detected significant embryonic lethality. All of the mutant late embryos and larvae examined lack tertiary branching of the tracheal system (data not shown), consistent with strong loss-of-function mutations at the *bs* locus (Guillemin *et al.* 1996). Examination of wings dissected from rare escapers that survive to the pharate adult stage revealed a tube wing phenotype identical to that found in known *bs* mutants (Montagne *et al.* 1996). Interestingly, during the course of four independent embryonic lethal-phase experiments with $bs^{E(br)292}$, 18% of the mutant animals showed embryonic lethality (Table 4), of which 29% of the dead embryos displayed dorsal anterior holes and several others showed aberrant head skeletons (data not shown). Likewise, $bs^{E(br)292}/Df(2R)Px2$ hemizygous animals show a similar degree of embryonic lethality and >25% of the dead embryos show head skeleton defects or dorsal anterior holes (data not shown). Since these phenotypes had not been reported previously, we also examined the strong loss-of-function bs^{k03267} allele; however, we did not recover any dead embryos exhibiting these phenotypes (data not shown). Additional experiments are required to determine if the novel embryonic phenotypes we observe in $bs^{E(br)292}$ mutants represent a stronger loss-of-function *bs* phenotype or an antimorphic or neomorphic phenotype associated with *bs* or are due to a closely linked second-site lethal mutation.

Lethal-phase analyses of the $sbd^{E(br)}$ mutations revealed that five of the six mutants are predominantly larval lethal, whereas $sbd^{E(br)228}$ shows some larval and pupal lethality with ~21% viable adults (Table 4). $sbd^{E(br)228}$ adults and adult escapers from *trans*-heterozygous combinations between $sbd^{E(br)228}$ and the other $sbd^{E(br)}$ alleles show the short, thick, and barbed bristles characteristic of mutations at the *Sb/sbd* locus (Figure 2B). Most of these adult escapers also display severely malformed legs (data not shown). Unexpectedly, we found that mutant animals from all six $sbd^{E(br)}$ alleles show defects in larval molting characterized by two complete sets of head skeleton. Occasionally, some cuticle from an earlier molt was found attached to the mouth hooks of dead mutant larvae (Figure 2D). $sbd^{E(br)48}$ and $sbd^{E(br)623}$ also display a unique phenotype characterized by excessive sclerotization of the anterior-most cuticle (Figure 2D). Interestingly, 9% of the dead embryos from $sbd^{E(br)48}$ and 19% of the dead embryos from $sbd^{E(br)623}$ show a dorsal anterior

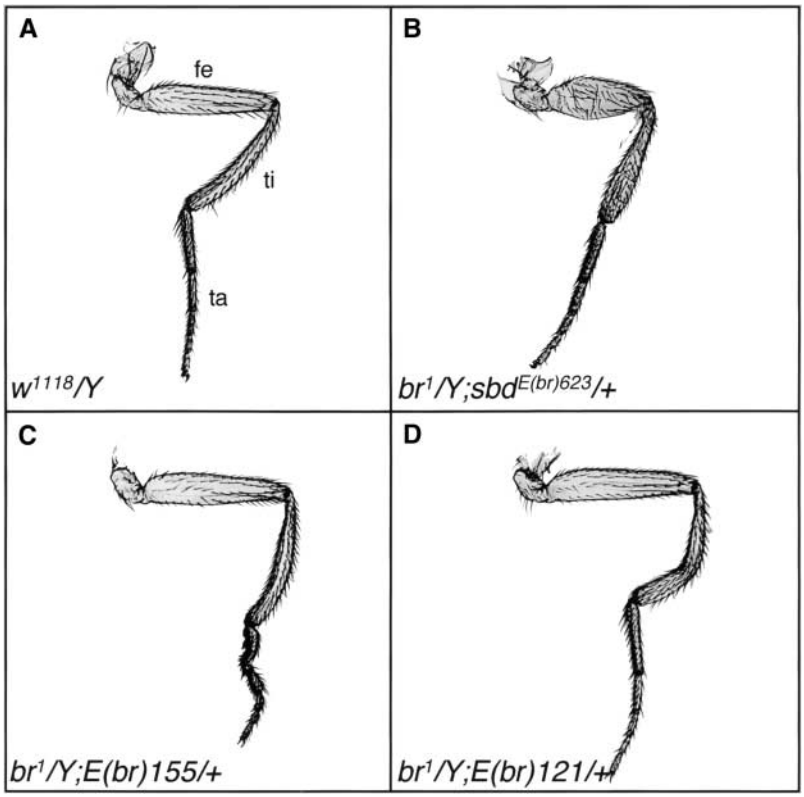

FIGURE 3.—Representative leg phenotypes of *E(br)* mutants. Brightfield photomicrographs are shown depicting cuticle preparations of adult legs from the third thoracic segment. (A) A w^{1118}/Y leg showing normal morphology. (B) A $br^{1}/Y;$ $sbd^{E(br)623}/+$ leg showing a short, fat femur and tibia. Fourteen of the *E(br)* mutations show this interaction phenotype. (C) A $br^{1}/Y;E(br)155/+$ leg showing bulbous and bent tarsal segments. *E(br)165* also shows this interaction phenotype. (D) A $br^{1}/Y;E(br)121/+$ leg showing a bent tibia. Four of the *E(br)* mutations show this interaction phenotype. Femur (fe), tibia (ti), and tarsal segments 1–5 (ta) are labeled.

hole similar to that seen with *Rho1* mutations (Figure 4D). These embryonic and larval phenotypes have not been described previously, although SPILLMAN and NOTHIGER (1978) reported early larval lethality in several *sbd* lines.

Characterization of the unidentified *E(br)* mutations revealed four mutant lines that display embryonic lethality characterized by defects in the midembryonic morphogenetic processes of dorsal closure and head involution (Table 4). *E(br)24*, *E(br)65*, and *E(br)155* mutants show 25, 14, and 97% embryonic lethality, respectively. In all three *E(br)* lines at least 10% of the dead embryos display a dorsal anterior hole similar to that found in $Rho1^{E(br)}$ mutants (compare Figure 4E with 4, B and C). In addition, we found that *E(br)155* and *E(br)165* mutants show a high penetrance of dorsal holes (Table 4 and Figure 4F). Specifically, nearly 50% of the *E(br)155* mutant embryos fail to complete dorsal closure (data not shown). Lethal-phase and phenotypic analyses of *E(br)165* revealed completely penetrant embryonic lethality characterized by a naked cuticle (data not shown). Because it was not possible to assess the terminal phenotype of *E(br)165* mutants using cuticle preparations, we resorted to indirect immunofluorescence analysis of late stage 17 embryos with an antibody directed against the septate junction marker Coracle (FEHON *et al.* 1994). Whereas their heterozygous siblings were resistant to the antibody due to the deposition of impermeable cuticle, the *E(br)165* mutant embryos showed robust Coracle staining revealing a highly penetrant dorsal open phenotype (Figure 4F).

SSNC analyses of *E(br)* mutations and mutations in Rho1 signaling genes: The similar embryonic lethal phenotypes seen in several *E(br)* and *Rho1* mutants raises the possibility that one or more of the genes affected by the *E(br)* mutations may function in a Rho1 signaling pathway. To examine this possibility, we conducted a series of SSNC experiments between the *E(br)* mutations and several alleles of genes known to function in Rho1 signaling, including *Rho1*, *RhoGEF2*, and *zip* (Table 5). The strong genetic interaction observed between the two $Rho1^{E(br)}$ alleles and mutations in *RhoGEF2* and *zip* serve as a useful control for these experiments and show that the Rho1 pathway is amenable to dose-sensitive genetic interaction studies (Table 5). In general, the $sbd^{E(br)}$ alleles display strong SSNC with $zip^{E(br)}$ and weak SSNC with *Rho1* alleles, although there is considerable allele-specific variation. Similar findings were observed by BAYER *et al.* (2003, this issue). In tests conducted with the unidentified *E(br)* mutations, we found that 6 of the 11 lines show >20% malformed legs in SSNC assays with at least one of the Rho1 pathway mutations (Table 5). Interestingly, all three of the unidentified *E(br)* mutants that display anterior open embryonic phenotypes show SSNC with *Rho1*. *E(br)65* also shows SSNC with *RhoGEF2* and *zip*. Finally, *E(br)121* and *E(br)444*

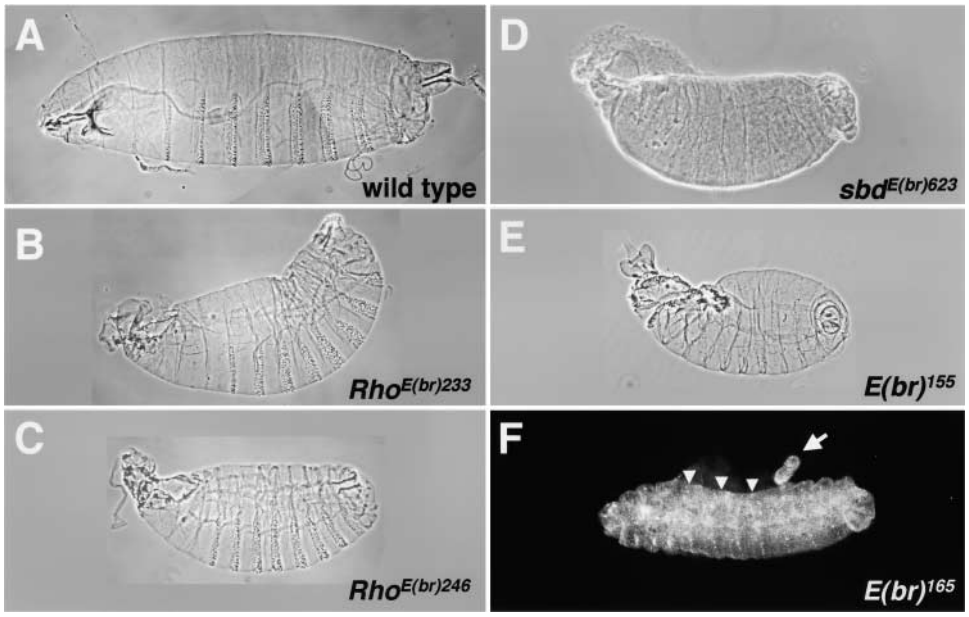

FIGURE 4.—Defective midembryonic morphogenetic events in *E(br)* mutants. Brightfield photomicrographs of cuticle preparations from (A) wild type, (B) $Rho^{E(br)233}$, (C) $Rho^{E(br)246}$, (D) $sbd^{E(br)623}$, and (E) *E(br)155* are shown. (F) Confocal optical section of an *E(br)165* mutant embryo stained with an antibody against the septate junction protein Coracle. All animals are shown with anterior to the left and dorsal up. (B and C) *Rho1* mutants show completely penetrant embryonic lethality characterized by a dorsal anterior open phenotype, indicative of a defect in head involution. Many *Rho1* mutants also show exaggerated curvature of the ventral surface caused by a mild defect in germband retraction. (D) More than 20% of $sbd^{E(br)623}$ mutants die as embryos, of which 19% display dorsal anterior holes. (E) *E(br)155* mutant animals show nearly completely penetrant embryonic lethality with ~10% of the embryos showing a dorsal anterior hole and ~50% showing a dorsal hole indicative of a defect in dorsal closure (not shown). (F) The head is completely involuted but the dorsal surface is not closed in *E(br)165* mutants as indicated by the sharp boundary of Coracle staining near the dorsal surface (arrowheads) and the extruded hindgut (arrow).

show very robust SSNC with alleles of all three Rho1 pathway genes tested and, although both of these mutations are semidominant, the strength of these interactions suggests that the corresponding genes likely function in a Rho1 pathway.

Transcription profiles of *br*[1]-interacting genes and Rho1 signaling pathway genes in wild-type and *br*[5] mutants: The central role of ecdysone signaling and *br* function in imaginal disc morphogenesis raises the possibility that one or more of the genes identified through our screens might be transcriptionally regulated by ecdysone and dependent on *br* activity. To test these possibilities, we analyzed the expression of genes identified through the *br*[1]-interacting screens as well as additional genes in the Rho1 signaling pathway in both wild-type and *br*[5] mutants. Total RNA was isolated from collections of ~100 hand-dissected leg imaginal discs per time point from staged *br*[5]*/Y* mid-third instar larvae and prepupae, as well as from their *Binsn/Y* siblings. The expression of *BR-C*, an ecdysone-inducible early gene, was used as a control to follow the timing of the late larval ecdysone pulse (Figure 5). Previous studies have demonstrated that all *BR-C* isoforms are induced as a primary response to ecdysone in imaginal discs and that *BR-C Z2*, *Z3*, and *Z4* isoforms are expressed at the beginning of the ecdysone peak, while the strongest expression of *BR-C Z1* is delayed several hours coincident with a reduction in the expression of *Z2*, *Z3*, and *Z4* (BAYER *et al.* 1996). The expression profile of the *BR-C* isoforms indicates that the discs respond to the late larval ecdysone pulse, although a slight developmental delay is detected in *br*[5] mutant discs where the shift from predominantly *Z2*, *Z3*, and *Z4* isoform expression to *Z1* occurs at +4 rather than at +2 (Figure 5). This delay in *br*[5] mutant discs was confirmed by monitoring the patterns of *EcR*, *E74*, and *E75* early gene transcription (data not shown). Previous work from APPEL *et al.* (1993) has shown that *Sb/sbd* transcription is dependent on ecdysone. The expression of *Sb/sbd* that initiates between −4 and 0 hr and peaks from +2 to +4 hr in control leg imaginal discs supports their findings (Figure 5). Interestingly, however, *Sb/sbd* transcription is unaffected by the *br*[5] mutation, showing only the ~2-hr developmental delay described above. In similar Northern blot experiments using RNA collected from whole animals and pooled leg and wing imaginal discs, we found that *Rho1*, *RhoGEF2*, *Rho kinase*, and *bs* are expressed in imaginal discs, that the level of expression of each gene remains constant from −18 to +6 hr, and that the expression of these genes is unaffected in *br*[5] mutant whole animals (data not shown).

We also examined the pattern of *ImpE3* transcription in control and *br*[5] leg imaginal discs in an effort to test for a possible regulatory interaction between *br* and *ImpE3* suggested by the deficiency screen results described above. In control leg imaginal discs, *ImpE3* expression begins ~4 hr before puparium formation, peaks at 2–4 hr after pupariation, and begins to subside by +6 hr (Figure 5). Interestingly, this expression is substantially reduced in *br*[5] leg imaginal discs, indicating that the *ImpE3* expression is dependent upon *br* function in this tissue.

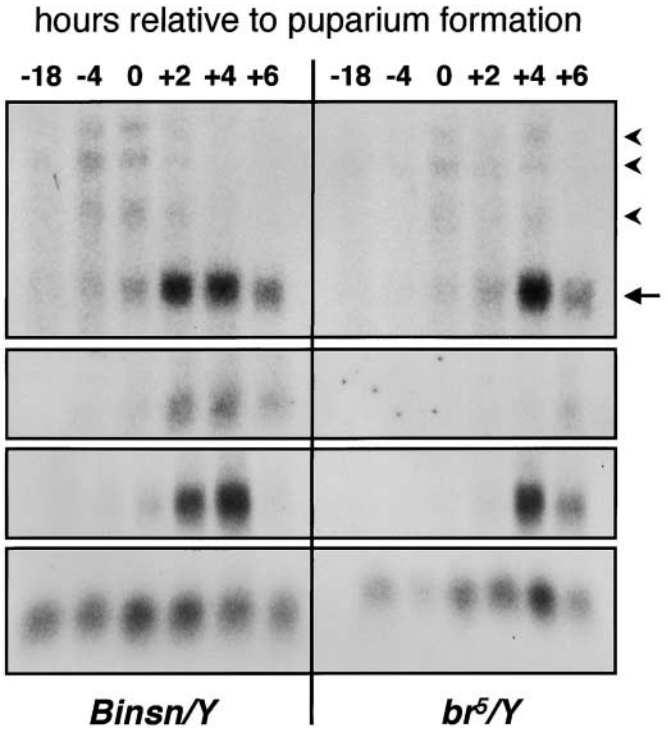

FIGURE 5.—*ImpE3* transcription, but not that of *Sb/sbd*, is dependent upon *br* function. Total RNA isolated from collections of staged *Binsn/Y* (control) and br^5/Y leg imaginal discs was fractionated by formaldehyde agarose gel electrophoresis and analyzed by Northern blot hybridization. The time in hours relative to puparium formation is depicted at the top. Hybridization to detect *BR-C* mRNA isoforms (*BR-C Z1* isoform is indicated by an arrow; *BR-C Z2*, *-Z3*, and *-Z4* isoforms are indicated by arrowheads) was used to follow changes in ecdysone titer. Hybridization to detect *rp49* mRNA was used as a control for loading and transfer. The br^5/Y −4-hr RNA sample is underloaded relative to the other samples.

DISCUSSION

Detailed studies over the past decade have focused on understanding how the imaginal discs undergo proliferation and pattern formation during larval development. In contrast, we know little about how the mature imaginal discs are transformed into their corresponding adult structures during metamorphosis—structures that bear no physical resemblance to the imaginal discs from which they were derived. This study is aimed at addressing this topic by focusing on the ecdysone-dependent morphogenesis of the adult leg in Drosophila.

Two screens for dominant enhancers of the br^1 malformed leg phenotype: We conducted two large-scale genetic modifier screens as a first step toward identifying novel links between the ecdysone signal and the cytoskeletal components that drive Drosophila leg morphogenesis. Both approaches took advantage of a hypomorphic mutation in the ecdysone-inducible *br* early gene, screening for enhancement of a rare malformed leg phenotype in adult flies. Screening through >750 stocks bearing either a chromosomal deficiency or a specific mutation, we identified nine loci on the second chromosome and eight loci on the third chromosome that interact with br^1. In a complementary F_1 screen of EMS-treated br^1 animals, we obtained 26 enhancer lines of which 20 were analyzed in detail. From these screens combined, we identified *Rho1, bs*, *sbd*, and *cTm* as br^1-interacting genes.

Conducting both a deficiency-based screen and a random mutagenesis screen allowed us to play the strengths of one approach off the weakness of the other. While a deficiency-based screen can quickly map br^1-interacting loci, it can be difficult to subsequently identify specific mutations to account for those interactions. On the other hand, an EMS screen rapidly generates specific br^1-interacting mutations, but significantly more effort is required to map and clone the corresponding gene. Here, we used complementation analyses between br^1-interacting deficiencies and EMS-induced mutations to identify br^1-interacting genes. Both screening strategies identified mutations in *Rho1* and *bs*. We also found an unidentified *E(br)* mutation that fails to complement a br^1-interacting deficiency. Moreover, further complementation tests between the *E(br)* mutations and mutations in previously identified br^1-interacting genes allowed us to identify six EMS-derived mutations as new alleles of *Sb/sbd*.

The results of our screens indicate that we have not yet begun to approach saturation in this pathway. Although we identified six alleles of *sbd* and two alleles of *Rho1* from the EMS screen, we also identified 12 mutations that are each represented by a single allele. In addition, we found at least 14 br^1-interacting loci by deficiency screening for which we did not recover an EMS-derived mutation. Principally, these results illustrate the complexity of imaginal disc morphogenesis and suggest that many genes are required to ensure the fidelity of this process. It is apparent that a larger screen will generate additional br^1-interacting mutations, some of which might map to genomic intervals identified through the deficiency screen.

A central role for Rho1 signaling in ecdysone-triggered leg disc morphogenesis: The identification of *Rho1* mutations as dominant enhancers of br^1, as well

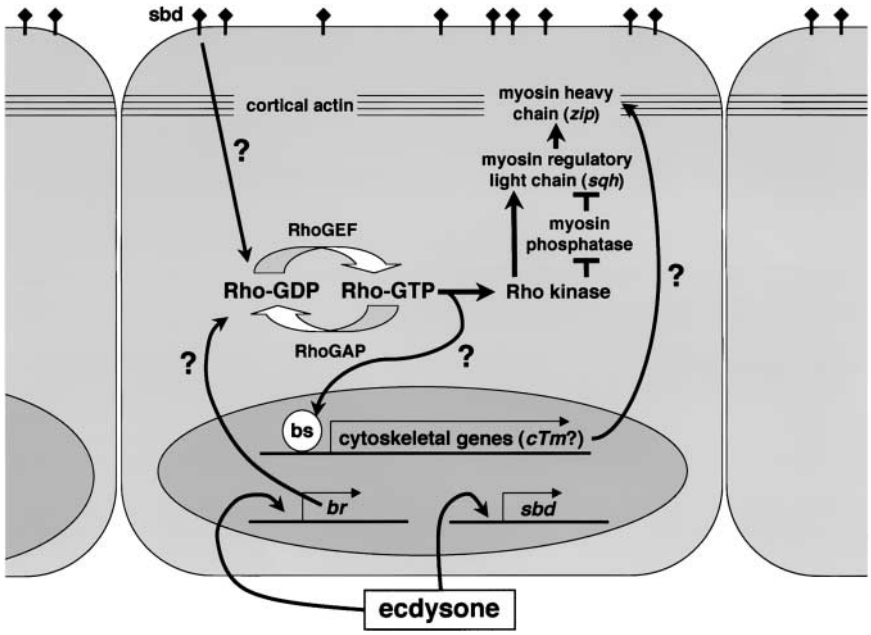

FIGURE 6.—Model of the signaling events that direct leg imaginal disc morphogenesis. Activation of Rho1 to the GTP-bound state plays a central role in directing the cell shape changes that drive disc morphogenesis. Possible regulatory interactions are represented by question marks. See text for details.

as the genetic interactions we observe between *E(br)* alleles and mutations in the Rho1 signaling pathway, indicate a central role for Rho1 in directing leg morphogenesis at the onset of metamorphosis (Figure 6). Signaling through the Rho1 small GTPase depends on a shift in the cellular equilibrium between inactive Rho-GDP and active Rho-GTP (reviewed in VAN AELST and D'SOUZA-SCHOREY 1997). This equilibrium is influenced by guanine nucleotide exchange factors (GEFs) that activate Rho1 by removing GDP from inactive Rho1 molecules, thereby allowing Rho1 to bind GTP. Countering this action, GTPase activating proteins (GAPs) stimulate the weak GTPase activity of Rho1. A key effector of activated Rho1 is Rho kinase, a serine/threonine kinase that regulates contractile events at the actin cytoskeleton. Rho kinase exerts its effect by phosphorylating and thereby inactivating the myosin-binding subunit of the myosin phosphatase complex. The principal substrate for myosin phosphatase is myosin regulatory light chain—a component of the actin cytoskeleton that can also be directly phosphorylated by Rho kinase. Therefore, the net effect of activating Rho kinase is to maintain the phosphorylated state of myosin regulatory light chain, which, in turn, results in the activation of the myosin heavy chain, allowing myosin complexes to move along actin filaments.

Over the past several years, genetic, molecular, and pharmacological perturbations of Rho1 signaling have revealed key roles for this signaling cascade in directing a variety of morphogenetic processes, including embryonic elongation in *Caenorhabditis elegans* and neural tube closure in the mouse (WISSMANN *et al.* 1997, 1999; BROUNS *et al.* 2000; WEI *et al.* 2001). In Drosophila, Rho1 signaling is required for cellularization of the blastoderm embryo, gastrulation, dorsal closure, head involution, neural development, and the establishment of planar polarity (reviewed in SETTLEMAN 2001). Recently, HALSELL *et al.* (2000) found that mutations in *Rho1* enhance the malformed leg phenotype associated with heterozygous *zip* mutations, suggesting a role for Rho1 in imaginal disc morphogenesis. Here we confirm and extend their observations by linking several Rho1 signaling components to the genetic functions of an ecdysone-inducible transcription factor, suggesting that ecdysone activation of the Rho1 signaling pathway may drive the cell shape changes associated with leg disc morphogenesis.

Genetic studies indicate that at least five components of the Drosophila Rho1 signaling cascade are required during imaginal disc morphogenesis: Rho1, RhoGEF2, myosin phosphatase, myosin regulatory light chain (encoded by *spaghetti squash* or *sqh*), and nonmuscle myosin heavy chain (encoded by *zip*; Figure 6). First, we found that deficiencies that uncover the *Rho1* locus as well as specific mutations in *Rho1* enhance the malformed leg phenotype associated with the br^1 mutation (Table 2). We also recovered two new alleles of *Rho1* as *E(br)* mutations from our EMS mutagenesis screen (Table 3). Second, we found strong SSNC between both $Rho1^{E(br)}$ alleles and $RhoGEF2^{11\text{-}3}$ (Table 5), suggesting that *RhoGEF2* is playing a pivotal role in activating *Rho1* during imaginal disc morphogenesis. Consistent with this observation, BAYER *et al.* (2003, this issue) detected strong SSNC between the same allele of *RhoGEF2* and three additional alleles of *Rho1*, and HALSELL *et al.* (2000) reported SSNC between three independent alleles of *RhoGEF2* and $zip^{E(br)}$. At least 20 potential *RhoGEF* genes are present in the Drosophila genome (SETTLEMAN 2001), however, raising the possibility that other RhoGEFs may also contribute to Rho1 activation during imaginal disc morpho-

genesis. Third, Mizuno *et al.* (2002) demonstrated that mutations in the myosin-binding subunit of *myosin phosphatase* can ameliorate the malformed wing phenotype associated with $zip^{E(br)}/zip^{02957}$ mutants and also reduce the penetrance of malformed wings in animals displaying SSNC between $zip^{E(br)}$ and mutations in *Rho1*, *RhoGEF2*, and *Rho kinase*. Fourth, the $zip^{E(br)}$ allele of nonmuscle myosin strongly enhances the malformed leg phenotype of br^{1} (Gotwals and Fristrom 1991) and displays robust SSNC with several alleles of *Rho1* and *RhoGEF2* (Halsell *et al.* 2000). Finally, malformed leg and wing phenotypes are seen in *sqh* mutants (Edwards and Kiehart 1996). Taken together, these studies provide strong evidence of a key role for Rho1 in directing the cell shape changes that drive imaginal disc morphogenesis (Figure 6).

In addition to direct effects on the actin cytoskeleton, Rho1 signaling can also transduce extracellular signals to the nucleus by activating SRF transcription factors. The mechanism of Rho1-dependent SRF activation is poorly understood but appears to require at least one of several Rho1-specific effector molecules, including Rho kinase, LIM kinase, and formin-homology proteins of the mDia family, in a cell-type-specific manner (Geneste *et al.* 2002). A current model proposes that the coordinated effects of these Rho1 effector molecules is to increase F-actin assembly and reduce F-actin severing, thereby decreasing the cytoplasmic pool of G-actin, which promotes the nuclear accumulation of MAL, an SRF coactivator (Sotiropoulos *et al.* 1999; Geneste *et al.* 2002; Miralles *et al.* 2003). Transcriptional targets of activated SRF include α- and β-actin, vinculin, and tropomyosin (Gineitis and Treisman 2001; Mack *et al.* 2001; Nakamura *et al.* 2001). In this context, Rho1-dependent transcriptional activation of SRF appears to be reinforcing the direct effects that Rho1 is producing on the actin cytoskeleton. It is intriguing then that we identified mutations in *bs* (the Drosophila ortholog of SRF) and *cTm* as dominant modifiers of br^{1} for leg disc morphogenesis, suggesting that a transcriptional pathway downstream of Rho1 is also important for this morphogenetic process and that *cTm* may be a transcriptional target of *bs* (Figure 6). Consistent with these ideas, Halsell and Kiehart (1998) identified *cTm* in an SSNC screen with $zip^{E(br)}$ using a similar malformed leg assay. We performed SSNC experiments between $bs^{E(br)292}$ and mutations in the Rho1 signaling pathway as an initial test for *Rho1*-dependent *bs* function during leg morphogenesis, but failed to detect any significant interaction (Table 5). Additional work will be required to assess the relative importance of the transcriptional effects of Rho1 signaling in imaginal disc morphogenesis.

Roles for ecdysone in directing leg disc morphogenesis: The identification of genetic interactions between members of the Rho1 signaling pathway and the ecdysone-inducible transcription factor encoded by *br* provides an intriguing tie between the steroid hormone and the cellular machinery that drives morphogenesis. To investigate whether members of the Rho1 pathway might be transcriptionally regulated by ecdysone, we examined the expression of *Rho1*, *RhoGEF2*, and *Rho kinase* in whole animals and imaginal discs dissected from staged late larvae and prepupae of both wild type and br^{5} mutants (data not shown). This study, however, revealed no changes in transcript levels in response to the late larval ecdysone pulse, and no effects of the amorphic br^{5} mutation on their expression (data not shown). It should be noted, however, that there are many possible targets for ecdysone regulation of Rho1 activity, including multiple RhoGEFs and RhoGAPs. Ecdysone may also be responsible for inducing the expression of one or more proteins required for the appropriate subcellular localization of the Rho1 complex, a level of regulation that is thought to be critical for its activation (reviewed in Symons and Settleman 2000). Possible targets for this regulation include a transmembrane protein that anchors Rho1 signaling components to the plasma membrane or a kinase that phosphorylates a RhoGEF to promote membrane association. The use of microarrays to identify ecdysone-inducible genes in imaginal discs would provide a powerful counterpoint to our genetic screens as well as a means of identifying these possible intermediates between the ecdysone and Rho1 signaling pathways.

Intriguingly, *Sb/sbd* represents the only known br^{1}-interacting gene that is induced directly by ecdysone in imaginal discs as they undergo morphogenesis (Figure 5; Appel *et al.* 1993). The function of the Sb/sbd type II transmembrane serine protease in this response, however, remains unknown. It has been suggested that Sb/sbd may direct localized proteolysis, breaking ties to the extracellular matrix at the apical cell surface and thereby facilitating disc elongation (von Kalm *et al.* 1995). Alternatively, *Sb/sbd* may contribute more directly to activation of the Rho1 pathway, as suggested by SSNC between *Sb/sbd* mutations and mutations in *Rho1*, *RhoGEF2*, *Rho kinase*, and *zip* (Table 5; Bayer *et al.* 2003, this issue). It is unlikely, however, that the ecdysone-directed expression of *Sb/sbd* is sufficient to promote all the events of leg disc morphogenesis. *Sb/sbd* expression is unaffected by the br^{5} mutation that completely blocks leg morphogenesis (Figure 5), indicating that a *br*-dependent, *Sb/sbd*-independent mechanism must contribute to normal leg development. In addition, *Sb/sbd* mRNA is first detectable in imaginal discs at puparium formation, several hours after the discs have initiated morphogenesis (Figure 5; Appel *et al.* 1993). Nevertheless, the frequency with which we recovered *sbd* alleles indicates that it is clearly an important part of this pathway, and future experiments should help to better define its role in leg morphogenesis.

It is interesting to note that most *sbd* mutants die during larval stages with molting defects (Figure 2D). This function for *sbd* has not been described previously

and provides an additional unexpected tie to ecdysone signaling. Ecdysone pulses during larval development trigger molting of the cuticle as the animal grows in size (Riddiford 1993). A key aspect of this response is the degradation of the old cuticle by proteases and chitinases that are secreted by the epithelium. It is possible that Sb/sbd contributes to these proteolytic activities during the molt. Alternatively, Sb/sbd may play a more general role in ecdysone signaling during the molts and at the onset of metamorphosis.

Finally, our Northern blot study provides the first observation of a *br*-dependent transcript expressed in imaginal discs, *ImpE3* (Figure 5). This gene is induced rapidly by ecdysone, is expressed primarily in imaginal discs, and encodes a secreted protein with a potential glycosylphosphatidylinositol anchor (Moore *et al.* 1990). Intriguingly, *ImpE3* lies within the 84D04 to 84F02 interval defined by three overlapping deficiencies that interact with br^1 (Table 1). It will be interesting to determine whether this genetic interaction can be attributed to *ImpE3*, providing a possible tie between ecdysone-regulated gene expression, *br* function, and leg disc morphogenesis.

Parallel ecdysone-triggered morphogenetic responses during embryogenesis and metamorphosis: Our EMS mutagenesis screen identified 11 *E(br)* mutations that appear to reside in unique genes and whose identities remain unknown. Seven of these mutations show SSNC with mutations in *Rho1*, *RhoGEF2*, or *zip* (Table 5), suggesting that the corresponding genes may function with *Rho1* to facilitate the cell shape changes that drive leg morphogenesis. Remarkably, although we originally isolated these mutations as dominant enhancers of br^1 during prepupal imaginal disc morphogenesis, we found that the zygotic loss-of-function phenotype for four of them included defects in embryonic morphogenetic events—head involution and dorsal closure (Table 4; Figure 4). Zygotic loss-of-function mutations in *Rho1* also show defects in head involution and dorsal closure (Figure 4, B and C; Magie *et al.* 1999), suggesting that these four *br*-interacting genes may be also be functioning with *Rho1* during these midembryonic morphogenetic processes.

Taken together, these observations raise the interesting possibility that a common ecdysone-directed, Rho1-mediated signaling cascade controls the morphogenetic movements that occur during two major developmental transitions in the life cycle, embryogenesis and metamorphosis. This idea fits with recent data that implicate a central role for ecdysone signaling in midembryonic morphogenetic events. A high titer pulse of ecdysone occurs midway through embryonic development, peaking from 6 to 12 hr after egglay, coincident with the morphogenetic movements of germband retraction, dorsal closure, and head involution (Kraminsky *et al.* 1980; Maróy *et al.* 1988). Mutations in *disembodied*, a gene that encodes a key steroidogenic enzyme required for ecdysone biosynthesis, result in defects in head involution and dorsal closure (Châvez *et al.* 2000). Similarly, disruption of *EcR* function in early embryos leads to highly penetrant defects in midembryonic morphogenetic movements (Kozlova and Thummel 2003). These observations have led to the proposal that ecdysone acts at two stages in the life cycle to trigger a dramatic change in morphology, establishing the basic body plan for the next stage in development—transforming the germband extended embryo with external head structures into a first instar larva or the third instar larva into an immature adult fly (Kozlova and Thummel 2003). The observation that four unidentified *E(br)* mutations and *Rho1*, identified solely by their effects on leg development, also play a role during embryonic morphogenesis, provides further support for this proposal and raises the interesting possibility that ecdysone directs morphogenesis during both embryogenesis and metamorphosis through a common Rho1-mediated pathway. It is interesting to note that one of these mutants, *E(br)165*, also displays defects in cuticle deposition, another phenotype that is shared in common with *disembodied* mutants and disruption of *EcR* function during embryogenesis (Châvez *et al.* 2000). Characterization of the genes disrupted by these *E(br)* mutations should provide further insights into this possible common regulatory pathway.

We thank S. Halsell, L. von Kalm, D. Kiehart, and the Bloomington Drosophila Stock Center for fly stocks and R. Fehon for the anti-Coracle antibodies used in this study. We are greatly indebted to J. Fristrom, L. von Kalm, and S. Halsell for stimulating conversations and sharing unpublished results. We thank P. Reid and J. Gallafant for technical assistance during part of this study. We also thank A. Bashirullah and T. Kozlova for critical comments on the manuscript. R.E.W. was supported as an Associate of the Howard Hughes Medical Institute and through a National Institutes of Health National Research Service Award. C.S.T. is an Investigator with the Howard Hughes Medical Institute.

LITERATURE CITED

Affolter, M., J. Montagne, U. Walldorf, J. Groppe, U. Kloter *et al.*, 1994 The *Drosophila* SRF homolog is expressed in a subset of tracheal cells and maps within a genomic region required for tracheal development. Development **120:** 743–753.

Andres, A. J., and C. S. Thummel, 1994 Methods for quantitative analysis of transcription in larvae and prepupae, pp. 565–573 in *Drosophila melanogaster: Practical Uses in Cell and Molecular Biology*, edited by L. Goldstein and E. Fryberg. Academic Press, New York.

Appel, L. F., M. Prout, R. Abu-Shumays, A. Hammonds, J. C. Garbe *et al.*, 1993 The *Drosophila Stubble-stubbloid* gene encodes an apparent transmembrane serine protease required for epithelial morphogenesis. Proc. Natl. Acad. Sci. USA **90:** 4937–4941.

Ashburner, M., 1989 *Drosophila: A Laboratory Manual.* Cold Spring Harbor Laboratory Press, Cold Spring Harbor, NY.

Ashburner, M., C. Chihara, P. Meltzer and G. Richards, 1974 Temporal control of puffing activity in polytene chromosomes. Cold Spring Harbor Symp. Quant. Biol. **38:** 655–662.

Baker, B. S., G. Hoff, T. C. Kaufman, M. F. Wolfner and T. Hazelrigg, 1991 The doublesex locus of *Drosophila melanogaster* and its flanking regions: a cytogenetic analysis. Genetics **127:** 125–138.

Bayer, C. A., B. Holley and J. W. Fristrom, 1996 A switch in *Broad-Complex* zinc-finger isoform expression is regulated posttranscriptionally during the metamorphosis of *Drosophila* imaginal discs. Dev. Biol. **177:** 1–14.

Bayer, C. A., S. R. Halsell, J. W. Fristrom, D. P. Kiehart and L. von Kalm, 2003 Genetic interactions between the *RhoA* and *Stubble-stubbloid* loci suggest a role for a type II transmembrane serine protease in intracellular signaling during Drosophila imaginal disc morphogenesis. Genetics **165:** 1417–1432.

Beaton, A. H., I. Kiss, D. Fristrom and J. W. Fristrom, 1988 Interaction of the *Stubble-stubbloid* locus and the *Broad-Complex* of *Drosophila melanogaster.* Genetics **120:** 453–464.

Belyaeva, E. S., M. G. Aizenzon, V. F. Semeshin, I. Kiss, K. Koczka *et al.*, 1980 Cytogenetic analysis of the 2B3–4–2B11 region of the X-chromosome of *Drosophila melanogaster.* I. Cytology of the region and mutant complementation groups. Chromosoma **81:** 281–306.

Birr, C. A., D. Fristrom, D. S. King and J. W. Fristrom, 1990 Ecdysone-dependent proteolysis of an apical surface glycoprotein may play a role in imaginal disc morphogenesis in *Drosophila.* Development **110:** 239–248.

Bocchinfuso, W. P., J. K. Lindzey, S. C. Hewitt, J. A. Clark, P. H. Myers *et al.*, 2000 Induction of mammary gland development in estrogen receptor-alpha knockout mice. Endocrinology **141:** 2982–2994.

Brouns, M. R., S. F. Matheson, K. Q. Hu, I. Delalle, V. S. Caviness *et al.*, 2000 The adhesion signaling molecule p190 RhoGAP is required for morphogenetic processes in neural development. Development **127:** 4891–4903.

Châvez, V. M., G. Marquâes, J. P. Delbecque, K. Kobayashi, M. Hollingsworth *et al.*, 2000 The *Drosophila* disembodied gene controls late embryonic morphogenesis and codes for a cytochrome P450 enzyme that regulates embryonic ecdysone levels. Development **127:** 4115–4126.

Condic, M. L., D. Fristrom and J. W. Fristrom, 1991 Apical cell shape changes during *Drosophila* imaginal leg disc elongation: a novel morphogenetic mechanism. Development **111:** 23–33.

D'Avino, P. P., and C. S. Thummel, 1998 *crooked legs* encodes a family of zinc finger proteins required for leg morphogenesis and ecdysone-regulated gene expression during *Drosophila* metamorphosis. Development **125:** 1733–1745.

DiBello, P. R., D. A. Withers, C. A. Bayer, J. W. Fristrom and G. M. Guild, 1991 The Drosophila *Broad-Complex* encodes a family of related proteins containing zinc fingers. Genetics **129:** 385–397.

Edwards, K. A., and D. P. Kiehart, 1996 *Drosophila nonmuscle myosin II* has multiple essential roles in imaginal disc and egg chamber morphogenesis. Development **122:** 1499–1511.

Erdelyi, M., A. M. Michon, A. Guichet, J. B. Glotzer and A. Ephrussi, 1995 Requirement for *Drosophila cytoplasmic tropomyosin* in *oskar* mRNA localization. Nature **377:** 524–527.

Fehon, R. G., K. Johansen, I. Rebay and S. Artavanis-Tsakonas, 1991 Complex cellular and subcellular regulation of notch expression during embryonic and imaginal development of *Drosophila*: implications for notch function. J. Cell Biol. **113:** 657–669.

Fehon, R. G., I. A. Dawson and S. Artavanis-Tsakonas, 1994 A *Drosophila* homologue of membrane-skeleton protein 4.1 is associated with septate junctions and is encoded by the *coracle* gene. Development **120:** 545–557.

Fekete, E., D. Fristrom, I. Kiss and J. W. Fristrom, 1975 The mechanism of evagination of imaginal discs of *Drosophila melanogaster.* II. Studies on trypsin-accelerated evagination. Wilhelm Roux's Arch. Dev. Biol. **173:** 123–138.

Fessler, L. I., M. L. Condic, R. E. Nelson, J. H. Fessler and J. W. Fristrom, 1993 Site-specific cleavage of basement membrane collagen IV during *Drosophila* metamorphosis. Development **117:** 1061–1069.

FlyBase, 1999 The FlyBase database of the Drosophila genome projects and community literature. Nucleic Acids Res. **27:** 85–88.

Fristrom, D., and J. W. Fristrom, 1975 The mechanism of evagination of imaginal discs of *Drosophila melanogaster.* I. General considerations. Dev. Biol. **43:** 1–23.

Fristrom, D., and J. W. Fristrom, 1993 The metamorphic development of the adult epidermis, pp. 843–897 in *The Development of Drosophila melanogaster*, edited by M. Bate and A. Martinez Arias. Cold Spring Harbor Laboratory Press, Cold Spring Harbor, NY.

Fristrom, J. W., W. R. Logan and C. Murphy, 1973 The synthetic and minimal culture requirements for evagination of imaginal discs of *Drosophila melanogaster* in vitro. Dev. Biol. **33:** 441–456.

Geneste, O., J. W. Copeland and R. Treisman, 2002 LIM kinase and Diaphanous cooperate to regulate serum response factor and actin dynamics. J. Cell Biol. **157:** 831–838.

Gineitis, D., and R. Treisman, 2001 Differential usage of signal transduction pathways defines two types of serum response factor target gene. J. Biol. Chem. **276:** 24531–24539.

Gotwals, P. J., and J. W. Fristrom, 1991 Three neighboring genes interact with the *Broad-Complex* and the *Stubble-stubbloid* locus to affect imaginal disc morphogenesis in Drosophila. Genetics **127:** 747–759.

Graves, B. J., and G. Schubiger, 1982 Cell cycle changes during growth and differentiation of imaginal leg discs in *Drosophila melanogaster.* Dev. Biol. **93:** 104–110.

Guillemin, K., J. Groppe, K. Ducker, R. Treisman, E. Hafen *et al.*, 1996 The *pruned* gene encodes the *Drosophila* serum response factor and regulates cytoplasmic outgrowth during terminal branching of the tracheal system. Development **122:** 1353–1362.

Halsell, S. R., and D. P. Kiehart, 1998 Second-site noncomplementation identifies genomic regions required for Drosophila nonmuscle myosin function during morphogenesis. Genetics **148:** 1845–1863.

Halsell, S. R., B. I. Chu and D. P. Kiehart, 2000 Genetic analysis demonstrates a direct link between rho signaling and nonmuscle myosin function during Drosophila morphogenesis. Genetics **155:** 1253–1265.

Karim, F. D., and C. S. Thummel, 1991 Ecdysone coordinates the timing and the amount of *E74A* and *E74B* transcription in *Drosophila.* Genes Dev. **5:** 1067–1079.

Kiss, I., A. H. Beaton, J. Tardiff, D. Fristrom and J. W. Fristrom, 1988 Interactions and developmental effects of mutations in the *Broad-Complex* of *Drosophila melanogaster.* Genetics **118:** 247–259.

Kozlova, T., and C. S. Thummel, 2003 Essential roles for ecdysone signaling during Drosophila mid-embryonic development. Science **301:** 1911–1914.

Kraminsky, G. P., W. C. Clark, M. A. Estelle, R. D. Gietz, B. A. Sage *et al.*, 1980 Induction of translatable mRNA for dopa decarboxylase in *Drosophila*: an early response to ecdysterone. Proc. Natl. Acad. Sci. USA **77:** 4175–4179.

Lefevre, G., 1976 A photographic representation and interpretation of *Drosophila melanogaster* salivary glands, pp. 31–66 in *The Genetics and Biology of Drosophila*, edited by M. Ashburner and E. Novitski. Academic Press, London.

Mack, C. P., A. V. Somlyo, M. Hautmann, A. P. Somlyo and G. K. Owens, 2001 Smooth muscle differentiation marker gene expression is regulated by RhoA-mediated actin polymerization. J. Biol. Chem. **276:** 341–347.

Magie, C. R., M. R. Meyer, M. S. Gorsuch and S. M. Parkhurst, 1999 Mutations in the *Rho1* small GTPase disrupt morphogenesis and segmentation during early *Drosophila* development. Development **126:** 5353–5364.

Mandaron, P., 1970 Dâeveloppement in vitro des disques imaginaux de la drosophile. Aspects morphologiques et histologiques. Dev. Biol. **22:** 298–320.

Maróy, P., G. Kaufmann and A. Dübendorfer, 1988 Embryonic ecdysteroids of *Drosophila melanogaster.* J. Insect Physiol. **34:** 633–637.

Martin, P., and I. Schneider, 1978 *Drosophila* organ culture, pp. 219–264 in *The Genetics and Biology of Drosophila*, edited by M. Ashburner and T. R. F. Wright. Academic Press, London.

Miralles, F., G. Posern, A. Zaromytidou and R. Treisman, 2003 Actin dynamics control SRF activity by regulation of its coactivator MAL. Cell **113:** 329–342.

Mizuno, T., K. Tsutsui and Y. Nishida, 2002 *Drosophila* myosin phosphatase and its role in dorsal closure. Development **129:** 1215–1223.

Montagne, J., J. Groppe, K. Guillemin, M. A. Krasnow, W. J. Gehring *et al.*, 1996 The *Drosophila* Serum Response Factor gene is required for the formation of intervein tissue of the wing and is allelic to *blistered.* Development **122:** 2589–2597.

Moore, J. T., D. Fristrom, A. S. Hammonds and J. W. Fristrom, 1990 Characterization of *IMP-E3*, a gene active during imaginal disc morphogenesis in *Drosophila melanogaster.* Dev. Genet. **11:** 299–309.

Nakamura, M., W. Nishida, S. Mori, K. Hiwada, K. Hayashi *et al.*, 2001 Transcriptional activation of beta-tropomyosin mediated by serum response factor and a novel Barx homologue, Barx1b, in smooth muscle cells. J. Biol. Chem. **276:** 18313–18320.

Natzle, J. E., A. S. Hammonds and J. W. Fristrom, 1986 Isolation of genes active during hormone-induced morphogenesis in *Drosophila* imaginal discs. J. Biol. Chem. **261:** 5575–5583.

Pino-Heiss, S., and G. Schubiger, 1989 Extracellular protease production by *Drosophila* imaginal discs. Dev. Biol. **132:** 282–291.

Poodry, C. A., and H. A. Schneiderman, 1971 Intercellular adhesivity and pupal morphogenesis in *Drosophila melanogaster*. Wilhelm Roux's Arch. Dev. Biol. **168:** 1–9.

Riddiford, L. M., 1993 Hormones and *Drosophila* development, pp. 899–940 in *The Development of Drosophila melanogaster*, edited by M. Bate and A. Martinez Arias. Cold Spring Harbor Laboratory Press, Cold Spring Harbor, NY.

Riddiford, L. M., P. Cherbas and J. W. Truman, 2000 Ecdysone receptors and their biological actions. Vitam. Horm. **60:** 1–73.

Robertson, C. W., 1936 The metamorphosis of *Drosophila melanogaster*, including an accurately timed account of the principal morphological changes. J. Morphol. **59:** 351–399.

Settleman, J., 2001 Rac 'n Rho: the music that shapes a developing embryo. Dev. Cell **1:** 321–331.

Sotiropoulos, A., D. Gineitis, J. Copeland and R. Treisman, 1999 Signal-regulated activation of serum response factor is mediated by changes in actin dynamics. Cell **98:** 159–169.

Spillman, E., and R. Nothiger, 1978 Cytology, genetics and lethality patterns of homozygous lethal mutations in the sbd region. Dros. Inf. Serv. **53:** 164–165.

Symons, M., and J. Settleman, 2000 Rho family GTPases: more than simple switches. Trends Cell Biol. **10:** 415–419.

Tata, J. R., 1999 Amphibian metamorphosis as a model for studying the developmental actions of thyroid hormone. Biochimie **81:** 359–366.

Tetzlaff, M. T., H. Jèackle and M. J. Pankratz, 1996 Lack of *Drosophila* cytoskeletal tropomyosin affects head morphogenesis and the accumulation of oskar mRNA required for germ cell formation. EMBO J. **15:** 1247–1254.

Thummel, C. S., 1996 Flies on steroids—*Drosophila* metamorphosis and the mechanisms of steroid hormone action. Trends Genet. **12:** 306–310.

Van Aelst, L., and C. D'Souza-Schorey, 1997 Rho GTPases and signaling networks. Genes Dev. **11:** 2295–2322.

von Kalm, L., D. Fristrom and J. Fristrom, 1995 The making of a fly leg: a model for epithelial morphogenesis. Bioessays **17:** 693–702.

Ward, R., P. Reid, A. Bashirullah, P. P. D'Avino and C. Thummel, 2003 GFP in living animals reveals dynamic developmental responses to ecdysone during *Drosophila* metamorphosis. Dev. Biol. **256:** 389–402.

Wei, L., W. Roberts, L. Wang, M. Yamada, S. Zhang *et al.*, 2001 Rho kinases play an obligatory role in vertebrate embryonic organogenesis. Development **128:** 2953–2962.

Wissmann, A., J. Ingles, J. D. McGhee and P. E. Mains, 1997 *Caenorhabditis elegans* LET-502 is related to Rho-binding kinases and human myotonic dystrophy kinase and interacts genetically with a homolog of the regulatory subunit of smooth muscle myosin phosphatase to affect cell shape. Genes Dev. **11:** 409–422.

Wissmann, A., J. Ingles and P. E. Mains, 1999 The *Caenorhabditis elegans* mel-11 myosin phosphatase regulatory subunit affects tissue contraction in the somatic gonad and the embryonic epidermis and genetically interacts with the Rac signaling pathway. Dev. Biol. **209:** 111–127.

Communicating editor: T. Schüpbach